JCB Journal of Cell Biology

REVIEW

Cytoskeletal organization of axons in vertebrates and invertebrates

Andreas Prokop

The maintenance of axons for the lifetime of an organism requires an axonal cytoskeleton that is robust but also flexible to adapt to mechanical challenges and to support plastic changes of axon morphology. Furthermore, cytoskeletal organization has to adapt to axons of dramatically different dimensions, and to their compartment-specific requirements in the axon initial segment, in the axon shaft, at synapses or in growth cones. To understand how the cytoskeleton caters to these different demands, this review summarizes five decades of electron microscopic studies. It focuses on the organization of microtubules and neurofilaments in axon shafts in both vertebrate and invertebrate neurons, as well as the axon initial segments of vertebrate motor- and interneurons. Findings from these ultrastructural studies are being interpreted here on the basis of our contemporary molecular understanding. They strongly suggest that axon architecture in animals as diverse as arthropods and vertebrates is dependent on loosely cross-linked bundles of microtubules running all along axons, with only minor roles played by neurofilaments.

Introduction

Axons are the cable-like processes of neurons that conduct nerve impulses and transmit this information at synapses to other cells. Axons can be up to 1 m long in humans and potentially up to 30 m long in blue whales (Smith, 2009). Axons are delicate structures, subject to enormous mechanical challenges imposed from the outside (e.g., bending and stretching through body movement) and the inside (e.g., axonal transport of large cargoes). In spite of these challenges, most axons cannot be replaced throughout an organism's lifetime, and mammals lose up to 40% of their axon mass toward high age (Calkins, 2013; Marner et al., 2003). Combatting such deterioration requires active maintenance mechanisms, and understanding them will provide new strategies to address the problem of axon loss in aging and disease (Hahn et al., 2019). To this end, we need detailed knowledge of axonal architecture.

An important property to be considered is that neurons and their axons can display substantial variations. For example, axon calibers can vary enormously between distinct neuron types (as detailed below); the need to minimize space and energy demand favors thin fibers, whereas the need to send information at high velocity and/or spike frequencies requires large-diameter fibers (Friede et al., 1984; Perge et al., 2009, 2012). Furthermore, neurons can be of different polarity (multipolar, unipolar, or pseudomonopolar), depending on their animal species of origin and functions as motorneurons, interneurons, or sensory neurons (Fig. 1 A); whether axon architecture needs to be adapted to these different morphologies remains an open question.

Neurons usually display lengthy axon shafts (light blue in Fig. 1 A) with a range of common features, including organelles, continuous networks of smooth ER, and an extensive cytoskeleton (Hahn et al., 2019). The axonal cytoskeleton of invertebrates and vertebrates alike shows conserved features, such as central longitudinal F-actin trails and cortical F-actin rings arranged by spectrins into a periodic pattern (Xu et al., 2013; Leterrier et al., 2017a). Of these, the actin rings seem to have important roles in regulating axonal stiffness (Krieg et al., 2017; Dubey et al., 2020), axon diameter (Costa et al., 2018, 2020) and microtubule (MT) polymerization (Qu et al., 2017). MTs of various lengths are organized into longitudinal parallel bundles that run along axons, often accompanied by intermediate filaments (neurofilaments [NFs]). MTs have a key role as the essential highways for axonal transport, as structural backbones of axons, and as the source of dynamic MTs that can contribute to morphogenetic processes such as axon branching (Hahn et al., 2019). But do MTs perform these functions based on common mechanistic or organizational principles that apply to the wide range of neuron types and axon diameters across the animal kingdom? To which degree can MT functions be replaced by NFs, which are abundant in some organisms and completely absent in others (Peter and Stick, 2015)?

School of Biology, Faculty of Biology, Medicine and Health, Manchester Academic Health Science Centre, The University of Manchester, Manchester, UK.

Correspondence to Andreas Prokop: andreas.prokop@manchester.ac.uk.

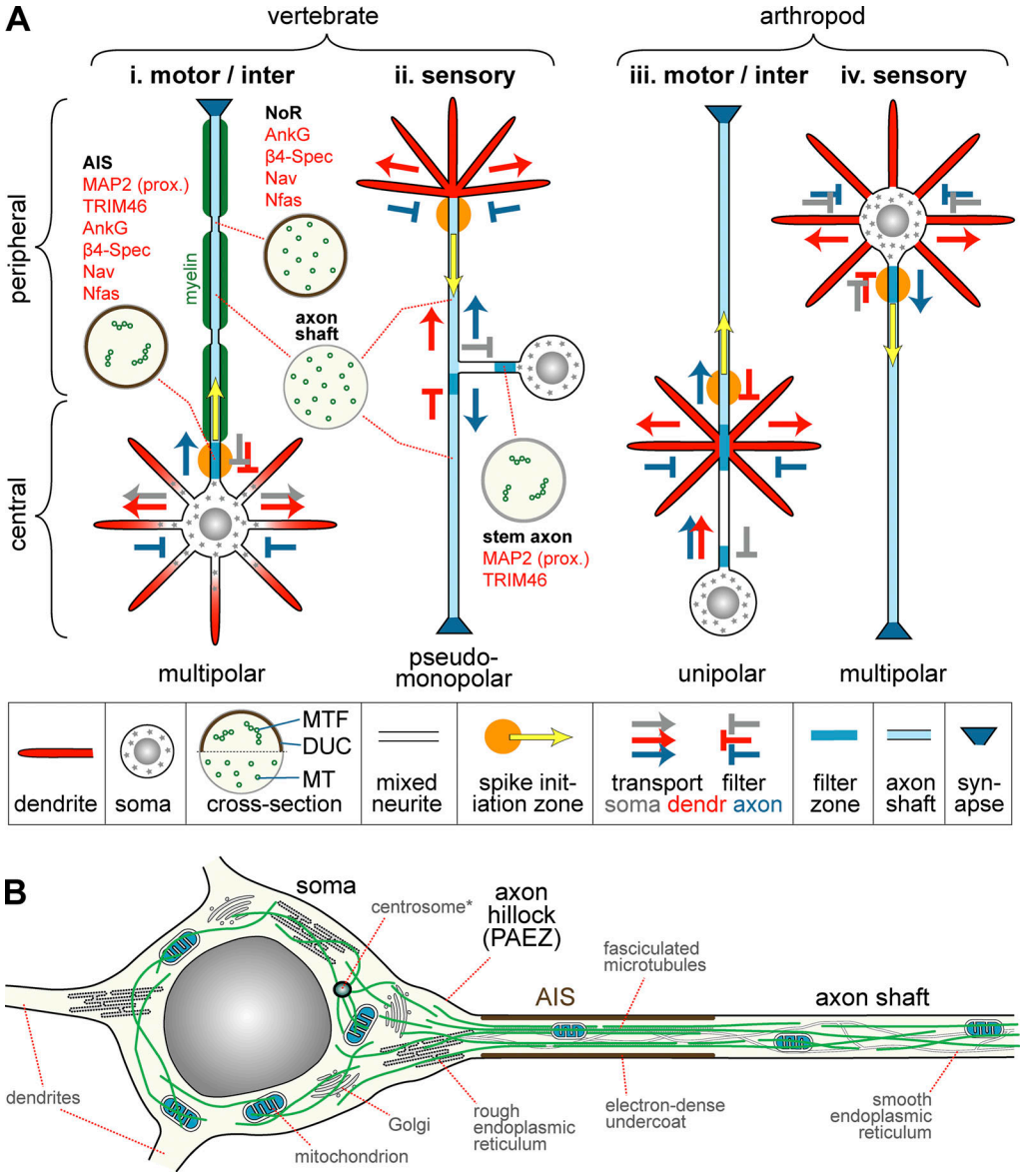

Figure 1. **Axonal compartments in different neuron types of vertebrates and arthropods. (A, i and iv)** Vertebrate motor-/interneurons (here shown with myelin sheath, green) and arthropod sensory neurons are bi- or multipolar; they can be expected to follow similar organizational principles, with transport of somatic, dendritic, and axonal materials (gray, red, and blue arrows, respectively) being decided mostly through exclusion mechanisms that reject somatic/dendritic materials (red and gray T's) at the base of axons and axonal materials at the base of dendrites (blue T); note that in sensory neurons of *Drosophila* also somatic materials are excluded from dendrites (gray T; Rolls, 2011). The axonal exclusion zone in the AIS of vertebrate motor-/interneurons coincides with the spike initiation zone (SIZ; orange circle; yellow arrow indicates direction of potential propagation), but little is known about this in arthropod sensory neurons. **(A ii)** Vertebrate sensory neurons (e.g., dorsal root or trigeminal ganglion cells) are pseudomonopolar (Nascimento et al., 2018). They are known to have an SIZ in the distal peripheral axon (Goldstein et al., 2019) and to filter somatic materials in the stem axon (gray T; Gumy et al., 2017); hypothetical filter zones should include barriers to dendritic materials at the entry point to the central axon (red T) and to axonal materials at the base of the peripheral dendrites (gray T). **(A iii)** Arthropod motor/interneurons are unipolar (Sánchez-Soriano et al., 2005); their axonal/dendritic filter zones are likely at the dendrite base (blue T) and the SIZ in the axon slightly peripheral to the dendrites (Burrows, 1996; Günay et al., 2015); the cell body is positioned away from that site and known to retain somatic materials, thus requiring a specific filter zone (gray T; Cohen, 1967). Circular insets show cross sections of different axonal compartments of vertebrate neurons (compare Figs. 2 and 4) illustrating the known MT distribution (small green circles; MTF, MT fascicles) and presence/absence of an electron-dense plasmalemma undercoat (DUC); the red text lists certain proteins present/absent at AISs and stem axons (see main text). Further abbreviations: β4-Spec, β4-spectrin; dendr, dendrite; Nav, voltage-gated sodium channels; Nfas, Neurofascin-186. Note that some neurons lack axons entirely (e.g., amacrine cells in the retina or granule cells in the olfactory bulb; Peters et al., 1991), whereas other axons can exist without their cell bodies (reported for ∼200-µm-long parasitic wasps; Polilov, 2012). **(B)** Soma and proximal axon of a typical vertebrate motor-/interneuron. In the cell body, MTs (green) are diffusely arranged; the axon hillock forms a transition zone where MTs are funneled toward the axon and somatodendritic organelles, including Golgi stacks and rough ER, are prevented from entering the axon (thus forming a PAEZ; Farías et al., 2015; Peters et al., 1991), whereas smooth ER networks continue along axons (Burton and Laveri, 1985; González and Couve, 2014; Tsukita and Ishikawa, 1976). In the AIS, MTs are fasciculated (see Fig. 2) and the plasmalemma forms an electron-dense undercoat. In the axon shaft, MTs form loose parallel arrangements (Bray and Bunge, 1981; Tsukita and Ishikawa, 1981). *Note that the centrosome has been reported to lose its MT nucleation function in neurons (Stiess et al., 2010).

To address these questions, modern superresolution imaging techniques provide us with powerful strategies (Leterrier et al., 2017a), but there are clear limitations. For example, resolving closely spaced MTs in axonal bundles still poses a challenge (Mikhaylova et al., 2015; Tas et al., 2017). Therefore, EM analyses remain pivotal. However, the bulk of existing EM studies (performed mainly on axons of vertebrates, to a lesser degree on invertebrates; see below) dates back to the final three decades of the last century. Those studies were interpreted with the very limited molecular and mechanistic knowledge existing at the time. This review will therefore revisit those publications and interpret classical structural findings in light of state-of-the-art molecular understanding. First, it will focus on axon initial segments (AIS; a specialized zone of the proximal axon in vertebrate motor- and interneurons; Fig. 1 B). It will then take a comparative look at the organization of MTs and NFs in the shafts of small- and large-caliber axons of vertebrate and invertebrate neurons to address whether and how different species of origin or size differences correlate with different concepts of axon architecture.

The AIS in vertebrate motor- and interneurons: Structure and molecular composition

To uphold the polarity of vertebrate inter- and motorneurons, components specific to the somatodendritic compartment have to be prevented from entering the axon (Fig. 1 Ai). This is thought to involve a staggered filter system including the axon hillock (referred to as the preaxonal exclusion zone [PAEZ]; Farías et al., 2015; details in Fig. 1 B) and the highly specialized AIS (see below); even the remainder of the axon shaft appears to display filter properties, as illustrated by microtubule-associated protein 2 (MAP2), which advances only poorly into the axon shaft if the AIS is abrogated (Jenkins et al., 2015).

The AIS is a specialization of vertebrate inter- and motorneurons that is tens of micrometers long and up to a few micrometers wide (Table S1), characterized by at least two prominent ultrastructural features reported consistently across different neuron types and animal species: parallel MT fascicles and a conspicuous electron-dense undercoat of the plasmalemma (Table S1; Fig. 1 B; and Fig. 2, A–D). According to EM studies of mitral cells in the mouse olfactory bulb, MT fascicles are not fully established until the end of embryogenesis and the dense undercoat not until days after birth (Hinds and Ruffett, 1973).

These AIS-specific structural features correlate with reports of proteins enriched at the AIS, usually appearing after axons have formed; they include the large cortical scaffold proteins AnkG (ankyrin-G) and nonerythrocytic β4-spectrin, filament-forming septins, the MT-binding ring-finger protein TRIM46 (tripartite motif–containing 46), the MT-binding factor EB3 (end-binding protein 3), the dynein regulator Ndel1 (neurodevelopment protein 1 like 1), the actin regulator Mical3 (molecule interacting with CasL), cell adhesion molecules such as neurofascin-186, and voltage-gated sodium channels and potassium channels; many of these components, as well as myosin 2 activity, were shown to contribute to AIS formation and maintenance (Berger et al., 2018; Fréal et al., 2019; Hamdan et al., 2020; Hedstrom et al., 2008; Jenkins et al., 2015; Kuijpers et al., 2016; Leterrier et al., 2017b; Salzer, 2019; Sobotzik et al., 2009). Several of these proteins can be clearly assigned to MT fascicles and/or electron-dense undercoat.

Thus, fasciculated MTs are connected via ∼25-nm-long electron-dense lateral bridges, thus forming sheath-like arrangements (curved arrows in Fig. 3 C) that appear like pearls on a string when analyzed in axonal cross sections (Fig. 2, A–D). The sizes of these fascicles are extremely variable, as illustrated by examples in Fig. 2, A–D that show between 2 and 23 MTs per fascicle (see also Palay et al., 1968). The electron-dense lateral bridges contain and require TRIM46 (Fig. 3 B), which is widely expressed in the nervous system (Harterink et al., 2019; van Beuningen et al., 2015). The MT–MT cross-linker MTCL1 (microtubule cross-linking factor 1) was shown to promote MT fascicle alignment; however, its role is restricted to the AIS of Purkinje cells (Satake et al., 2017), leaving open how MTCL1 functionally relates to TRIM46, which is likewise present in this cell type (van Beuningen et al., 2015).

The structure of the 35-nm-thick electron-dense undercoat was described in a three-layer model (Fig. 3 A; Chan-Palay, 1972) that agrees with various independent transmission EM (TEM) studies (Conradi, 1969; Kosaka, 1980a, 1980b; Nakajima, 1974). In its radial dimension, the TEM model matches well with a model based on superresolution microscopy of AIS-enriched proteins (Fig. 3 B; Leterrier et al., 2015). However, in the longitudinal dimension, both models diverge: the TEM model proposes a repetitive pattern with a periodicity of 60–80 nm (Fig. 3 A; arrowhead in Fig. 5 b of Nakajima, 1974); in contrast, numerous superresolution analyses have built a convincing case for a periodicity of ∼190 nm, which I could not find reflected in any TEM reports (Fig. 3 B; Huang and Rasband, 2018; Jacko et al., 2018; Jones and Svitkina, 2016; Leterrier, 2018; Leterrier et al., 2017a; Schlüter et al., 2019; Sohn et al., 2019). To explain this mismatch, refined EM studies will be required.

Functional roles of the AIS of vertebrate motor- and interneurons

50 yr ago, the MT fascicles at the AIS were discussed to be required for "protoplasmic streaming into the axon" and the dense undercoats for the "production of the electrical signal" (Palay et al., 1968). Today we know that AIS specializations help to filter somatodendritic components (preventing them from diffusing or being transported into axons) and establish the spike initiation zone (SIZ), where action potentials are initiated.

First, the AIS serves as a diffusion barrier for nonaxonal lipids and transmembrane proteins (Kobayashi et al., 1992; Nakada et al., 2003; Winckler et al., 1999), potentially requiring components of the dense undercoat such as cortical actin rings, AnkG, and β4-spectrin (Albrecht et al., 2016; Machnicka et al., 2014; reviewed in Huang and Rasband, 2018).

Second, the filtering of transported somatodendritic cargo at the AIS was proposed to involve actin patches or polarized actin networks, which are regulated by Mical3 and mediate the reversal of somato-dendritic cargo transport via the actin-based motor protein myosin-Va (Al-Bassam et al., 2012; Balasanyan et al., 2017; Hamdan et al., 2020; Lewis et al., 2009; Watanabe et al., 2012). This said, other studies have questioned the

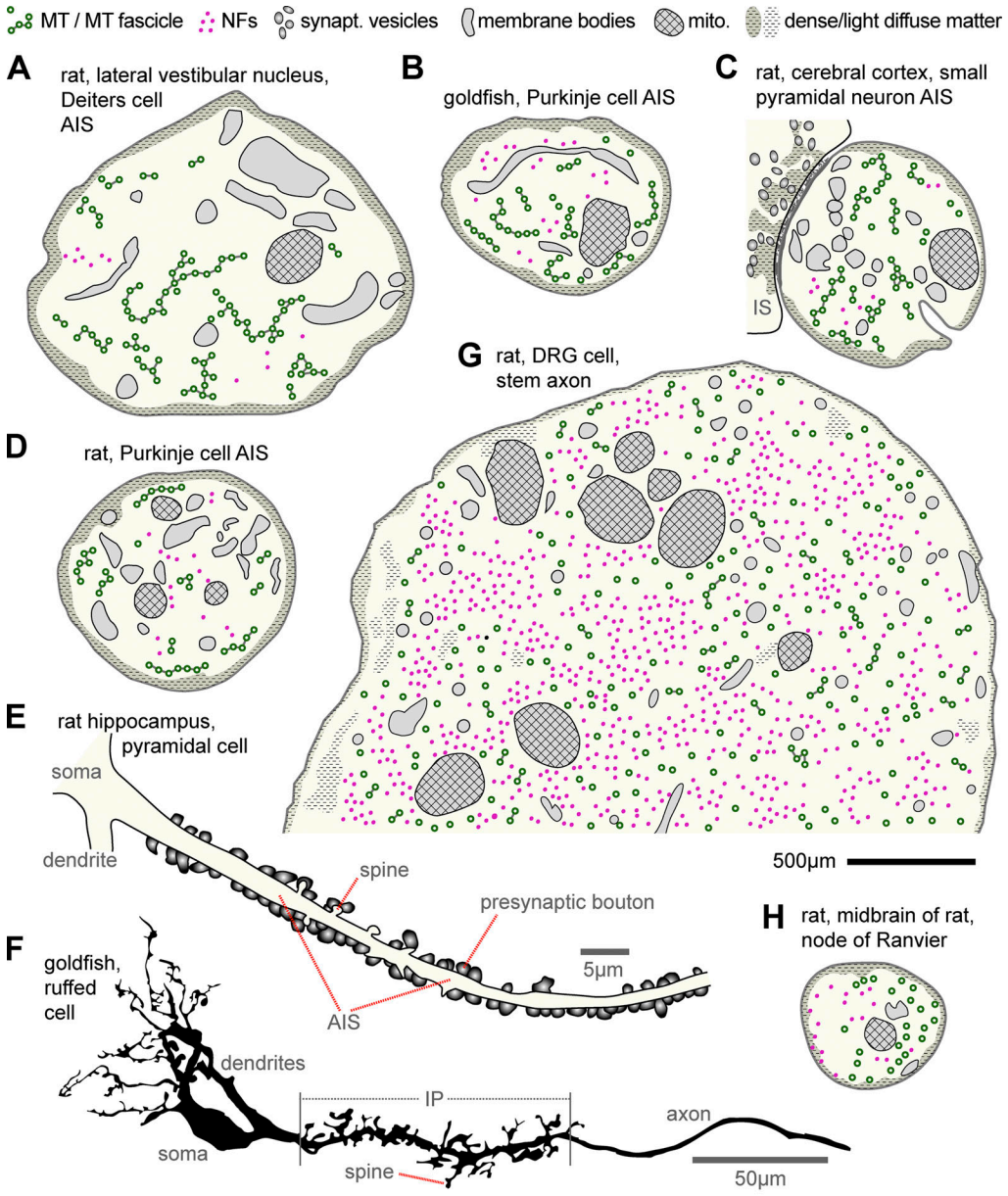

Figure 2. **Ultrastructural features at the AIS, stem axon, and NoRs. (A)** AIS of a giant cell of Deiters in the rat lateral vestibular nucleus (Palay et al., 1968). **(B)** AIS of a goldfish Purkinje cell (Matsumura and Kohno, 1991). **(C)** AIS of a small pyramidal neuron of the rat cerebral cortex (Peters et al., 1968) bearing an input synapse (IS), which is symmetric (thin postsynaptic undercoat) with flat pleiotropic vesicles. **(D)** AIS of a rat Purkinje cell (Chan-Palay, 1972). **(E)** Reconstruction from a TEM series of a pyramidal cell AIS with numerous presynaptic boutons and small spines in the rat hippocampus (redrawn from Kosaka, 1980a). **(F)** Initial unmyelinated portion (IP; proximal part of which is the AIS; see Table S1) of a ruffed cell in the frog olfactory bulb with numerous pre- and postsynaptic spines (redrawn from Kosaka and Hama, 1979b). **(G)** Stem axon of a DRG cell in rat (Nakazawa and Ishikawa, 1995). **(H)** NoR in the midbrain of rat (Peters, 1966). Note that NFs are sparse in AISs and that MTs are not fasciculated in NoRs. Best guesses were made with respect to structures drawn; scales in most original photos were given as magnifications (unfortunately meaningless in PDF format) and were estimated here by measuring MT diameters; the suggested black scale bar for A–D, G, and H represents 500 nm. Publications providing further examples of stem axons or NoRs are provided in the main text; for further AIS descriptions, see Table S1.

existence of adequate actin networks at the AIS (Jones et al., 2014; Jones and Svitkina, 2016). Alternatively or in addition, MT-based mechanisms were proposed that involve the selective activation of dynein-mediated retrograde transport through Ndel1 (Huang and Rasband, 2018; Leterrier, 2018; Kuijpers et al., 2016; Ye et al., 2020). Notably, both actin- and MT-based filtering mechanisms seem to involve a tug-of-war between motor proteins that pull in opposite directions, potentially strong enough to cause MT disorganization if thrown out of balance (Kuijpers et al., 2016). Such mechanical forces likely require a more stable architecture, potentially explaining why MTs arrange into tight fascicles at the AIS.

Furthermore, it has been shown that MTs at the AIS are anchored to the axonal surface through binding via EB3 to the tail domains of AnkG (Fig. 3 B; Fréal et al., 2019; Leterrier, 2018; Vassilopoulos et al., 2019); this interaction is essential for MT

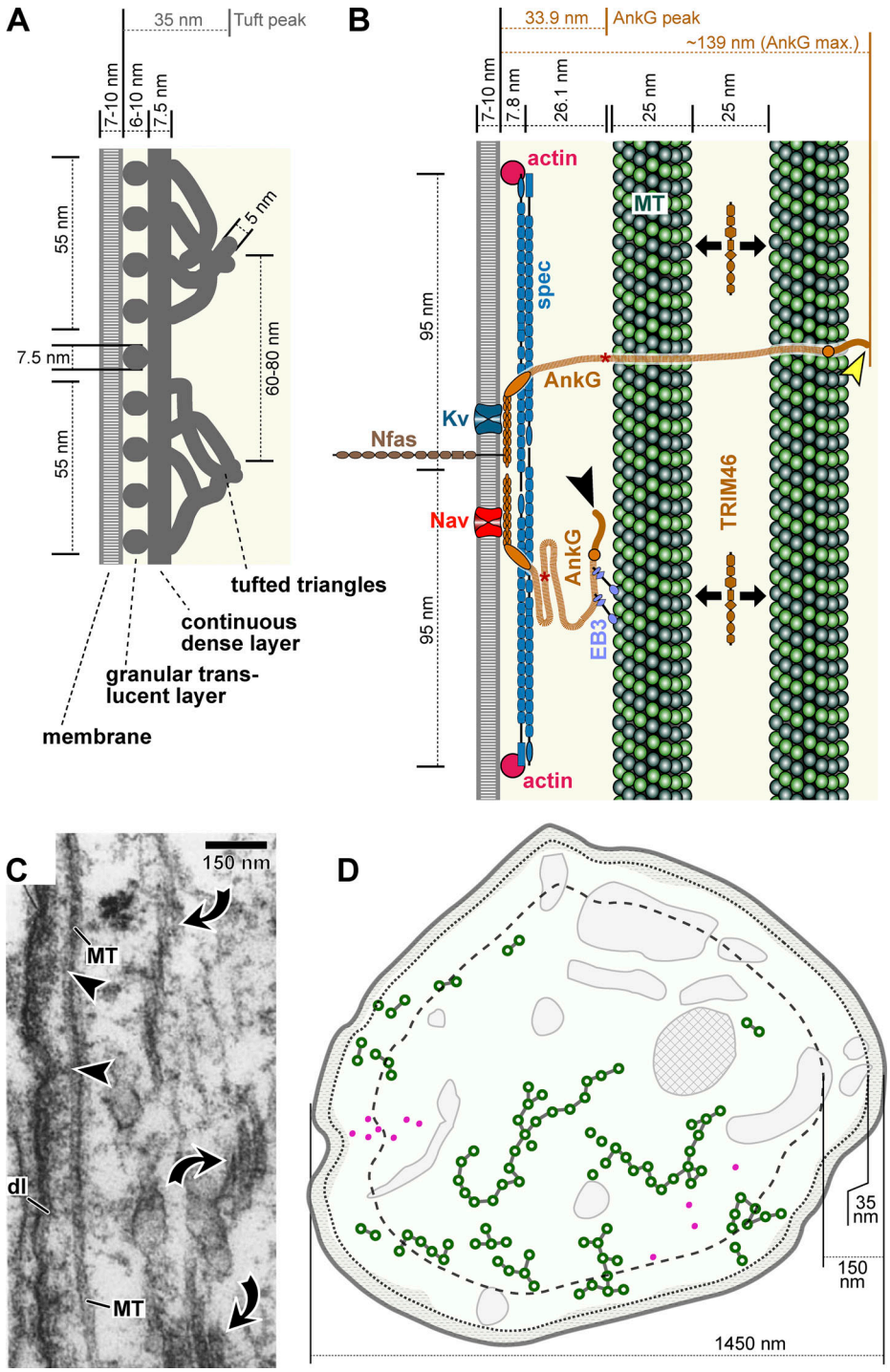

Figure 3. **Dimensions at the AIS.** Descriptions of the three-layered organization of the dense undercoat at the AIS viewed in longitudinal axon sections at either the ultrastructural (A; modified from Chan-Palay, 1972) or superresolution level (B; modified from Leterrier et al., 2015). The continuous dense layer may reflect spectrins (spec) separated ∼8 nm from the plasma membrane in both models. The tufted triangles composed of ∼5-nm-thick filaments likely correspond to the tails of AnkG (reported to be 4–7.5 nm thick also in platinum replica EM; Jones et al., 2014), with the position of their C-tail domains peaking at ∼35 nm beneath the membrane (black arrowhead in B), although a maximal stretch of ∼139 nm was reported (yellow arrowhead; Jones et al., 2014). Asterisks on the AnkG C-tail indicate the Ndel1 binding site (Ye et al., 2020). Granules in the translucent layer in A have currently no molecular explanation, although a subfraction of them might represent actin rings. For explanations regarding voltage-gated sodium/potassium channels (Kv/Nav) or neurofascin-186 (Nfas), see main text. **(C)** Original micrograph of a longitudinal axon section showing a MT in contact with the tufted layer of the dense undercoat (arrowheads; modified from Palay et al., 1968), suggesting that some MTs are in reach of AnkG; dl, dense layer (see A). Further MT bundles (curved arrows) appear to be out of reach even of the extended AnkG C-tail. **(D)** AIS cross section of a giant cell of Deiters in the rat lateral vestibular nucleus (Palay et al., 1968; same as in Fig. 2 A). The stippled/dashed lines indicate 35/150 nm distance from the plasma membrane (i.e., the peak/maximal distances of the AnkG C-tail shown in B) illustrating that many MT bundles are unlikely to be directly anchored to the axonal cortex.

fasciculation (Sobotzik et al., 2009). Furthermore, the dynein regulator Ndel1 binds to the AnkG tail (asterisks in Fig. 3 B), and this interaction is essential for AIS filter functions (Ye et al., 2020). In agreement with these functional studies, EM analyses suggest that a fraction of MTs are in contact with the undercoat (Fig. 3 C). However, many MT fascicles are positioned centrally in the axon, clearly out of reach of AnkG (Fig. 3 D). This raises the question as to whether only peripheral MT fascicles are involved in transport filtering and whether central MT fascicles drift freely in the axoplasm or are linked up via inconspicuous linkers that ultimately depend on AnkG.

Third, the AIS is a SIZ, meaning it triggers action potentials as the integrated outcome of supra-threshold depolarizations propagating from the somatodendritic compartment (Kole and Stuart, 2012). This function requires a well-balanced enrichment of voltage-gated sodium and potassium channels at the AIS (NaV and Kv in Fig. 3 B), which are likewise anchored via AnkG (Akin et al., 2015; Hefting et al., 2020). Importantly, neurons can fine-tune their excitability by changing the length of the AIS, the composition and posttranslational modification of ion channels, or the distance from the soma through mechanisms that involve calcium/calcineurin, MT stabilization, and myosin II (Berger et al., 2018; Bolós et al., 2019; Evans et al., 2015, 2017; Grubb and Burrone, 2010; Hatch et al., 2017; Kuba et al., 2010, 2014, 2015).

In various neuron types, the excitability at the AIS is also regulated by synapses in their majority inhibitory input synapses (Fig. 2, C and E; and Table S1). Their formation can be mediated by AnkG-dependent recruitment of the adhesion factor neurofascin-186 (Nfas in Fig. 3 B; Ango et al., 2004; Kriebel et al., 2011) and is regulated by synaptic activity (Pan-Vazquez et al., 2020). As listed in Table S1, many AIS descriptions highlight the occurrence of varicose spines of variable lengths and shapes (Fig. 2, E and F; see also Sobotzik et al., 2009) which seem to lack MTs and sometimes harbor more than one synapse. Beneath input synapses or spines the dense undercoat is consistently reported to be interrupted (Fig. 2 C), and many authors mention the presence of cisternal organelles (Table S1) that bear some resemblance with the spine apparatus (i.e., stacks of ER required for synaptic plasticity; Deller et al., 2003).

Do AIS features apply to other neuron classes?

In accordance with the polarity of vertebrate motor- and interneurons, the AIS is both a filter zone and a SIZ (Fig. 1 A, i). A similar combined compartment might be expected in the initial axon segment of arthropod sensory neurons (which have similar polarity; Fig. 1 A, iv), but not in vertebrate sensory neurons or arthropod motor- and interneurons (Fig. 1 A, ii and iii). Unfortunately, only few data are available for those neuron classes (legend of Fig. 1 A; Smarandache-Wellmann, 2016).

For example, sensory neurons of vertebrates (e.g., dorsal root ganglion [DRG] or trigeminal ganglion neurons) form a stem axon that then bifurcates into a central and peripheral axon arm (Fig. 1 A, ii; Nascimento et al., 2018). Stem axons display fasciculated MTs comparable to the AIS, whereas the electron-dense undercoat is absent (Fig. 2 G; Bird and Lieberman, 1976; Ishikawa et al., 1980; Peach, 1975; Zelená, 1971). Only one report mentions an extremely short (2–4 µm) stretch of membrane with an electron-dense undercoat (Zenker and Högl, 1976).

Consistent with the presence of MT fascicles and similar to the AIS, the stem axon displays TRIM46 and, proximal to it, MAP2 (Fig. 1 A, i versus Fig. 1 A, ii; Gumy et al., 2017; van Beuningen et al., 2015). These proteins may represent a staggered PAEZ/AIS-like filter system (see above), since MAP2 is required to block somatic organelles from entering DRG axons; in addition, MAP2 selectively activates kinesin-mediated transport, in line with a recently proposed "MAP code" for the regulation of polarized MT-based traffic (Gumy et al., 2017; Monroy et al., 2020); these roles of MAP2 demonstrated at stem axons may similarly contribute to PAEZ filter functions at the axon hillock. Outside the stem axon, vertebrate sensory neurons likely have further filter zones (Fig. 1 A, ii), but little is known at present.

Consistent with the lack of the electron-dense undercoat (Fig. 2 F), stem axons do not show enrichment of AnkG, β4-spectrin, or sodium channels (Fig. 1 A, i versus Fig. 1 A, ii; Gumy et al., 2017). This suggests that MT fascicles can form independently of AnkG and that stem axons have no SIZ functionality. Instead, electrophysiological studies have shown that the SIZ of DRGs is located in the peripheral axon, slightly removed from the dendritic compartment (Fig. 1 A, ii); similar to the AIS, this peripheral SIZ is dynamic and moves closer to the dendrites upon sensitization (Goldstein et al., 2019). Whether it displays AnkG expression and/or an electron-dense undercoat remains to be seen.

Nodes of Ranvier (NoRs) are the small unmyelinated segments along myelinated axons required for saltatory conduction (Fig. 1 A, i). NoRs display AIS-like undercoats (15–25 nm thick, 5–10 nm separated from plasmalemma) but no obvious MT fasciculation (Fig. 2 E; Conradi and Skoglund, 1969; Waxman et al., 1972; Elfvin, 1961; Kosaka, 1980b; Peters, 1966; Reles and Friede, 1991; Tsukita and Ishikawa, 1981; p. 104 and 260ff. in Peters et al., 1991). Only the most proximal NoRs in DRG neurons seem to display MT fascicles, potentially due to spillover of cross-linkers from the stem axon (Nakazawa and Ishikawa, 1995). Ethanolic phosphotungstic acid (an anionic heavy metal complex known to label basic proteins at synaptic densities; Jones, 1993) was reported to label the undercoats at both NoR and AIS, suggesting molecular commonalities (Sloper and Powell, 1973, 1979). We now know that NoRs lack TRIM-46, consistent with the absence of MT fasciculation (van Beuningen et al., 2015) but express characteristic AIS proteins consistent with the dense undercoat and excitability of NoRs, including AnkG, β4-spectrin, neurofascin-186, Nr-CAM, and high levels of voltage-gated sodium channel (Fig. 1 A, i; Kordeli et al., 1995; Dzhashiashvili et al., 2007; Yang et al., 2007; Liu et al., 2020). A further site where AIS-like undercoats were shown to correlate with the expression of at least AnkG are the "hot spots" in dendrites of the rat olfactory bulb (Kosaka et al., 2008).

Taken together, key features coinciding at the AIS can occur in separation in other neuron types or compartments. Therefore, using the term AIS for neurons other than vertebrate motor- or interneurons might be misleading; filter zones, diffusion barriers, or SIZs are expected to be distributed differently

in neurons of other polarity (Fig. 1 A), and whether their molecular mechanisms match those at the AIS remains to be seen.

The numbers and lengths of axonal MTs vary as a function of neuron type and organism

The axon shaft is the longest neuronal compartment and can display enormous structural variations (Table S2). With regard to the length of axonal MTs, it was originally believed that all axonal MTs extend from the soma. This was supported by studies in rat sensory and motor fibers showing that MT numbers of the main axon are equal to the added numbers of its daughter neurites, as if MTs at branch points merely decide whether to continue into one or the other branch (e.g., Weiss and Mayr, 1971a). This view was disputed by other findings: for example, in certain rat and crayfish motorneurons, the sum of cross-sectional areas of daughter branches was found to increase up to ∼10-fold, accompanied by substantial increases in MT counts (Nadelhaft, 1974; Zenker and Hohberg, 1973). This clearly indicated that new MTs arise within the axon, and we now know that nucleation, the seeding of new MTs, occurs in the axon shaft (Baas and Ahmad, 1992; Sánchez-Huertas et al., 2016; Stiess et al., 2010). Anchoring mechanisms that orient nucleation events toward the axon tip (Cunha-Ferreira et al., 2018) ensure that MTs have a consistent parallel polarity in axons (Baas et al., 1988; Baas and Lin, 2011; Yau et al., 2016).

Little data are available describing the actual lengths of MTs in axons. From serial TEM analyses of fairly short axon fragments, a range of MT lengths was estimated as follows: 430 µm/97 µm (frog, olfactory axons in the olfactory nerve/olfactory bulb; Burton, 1987), 108 µm (rat, cultured sensory nerves; Bray and Bunge, 1981), 513–757 µm/374 µm (mouse, internodal/nodal regions of sensory saphenous nerve; Tsukita and Ishikawa, 1981) and 9–23 µm/∼5 µm/∼6.5 µm (*Caenorhabditis elegans*, mechanosensory axons/axons of GABAergic dorsal D-type neurons/other axons; Chalfie and Thomson, 1979; Kurup et al., 2015). In agreement with the EM data for *C. elegans*, advanced live imaging strategies reported ∼6-µm-long MTs in axons of DA9 motorneurons (Yogev et al., 2016). Serial TEM analyses in both *C. elegans* and rat also reported the direct observation of very short MTs (1–4 µm), which might represent MT fragments undergoing transport (Baas, 2002; Baas et al., 2006). Notably, developing rat hippocampal neurons in culture overwhelmingly showed short fragments (range, 0.05–40 µm; average, 4 ± 5 µm; Yu and Baas, 1994), which might reflect high MT dynamics at the axon growth stage.

The length of MTs potentially impacts axonal transport dynamics (Yogev et al., 2016), but likely more important is the number and density of MTs, which, according to mathematical modeling, correlates with transport volume (Wortman et al., 2014). This has been most convincingly studied in DRG neurons (Fig. 1 A, ii), where the peripheral axon branch has a larger caliber, displays more MTs, and has a higher transport rate than is observed in the central branch of the same neurons (reviewed in Nascimento et al., 2018).

Across the animal kingdom, axon diameters were reported to be in the range of 0.1 to 30 µm in vertebrates, 0.1 to >100 µm in arthropods (giant axons of some spiders, crustaceans, and cockroaches; Castel et al., 1976; Foelix and Troyer, 1980; Nadelhaft, 1974), and up to a millimeter in squid (as the result of axonal fusion of 300–1,500 neurons; Young, 1936; Brown and Lasek, 1990). For axons of vertebrates and arthropods, MT numbers per profile area range between 1 and >250,000 MTs and their densities between 2 and ∼100 MTs/µm^2 (Table S2), with a reported outliers far above 100 (Fadić et al., 1985).

In light of these enormous ranges, the question arises as to whether the architectural challenges posed by different axon diameters require specific solutions or can be accommodated by common organizational concepts.

In small-caliber axon shafts of vertebrate and invertebrates, MTs are spaced by MAPs

Small-caliber axons (<300 nm diameter) can be found in most species (Fig. 4, A, B, G, and H), for example the olfactory bulb or the molecular layer of the cerebellum of vertebrates (Andres, 1965a; Harada et al., 1994; Kreutzberg and Gross, 1977; Peters et al., 1991), peripheral nerves and the ventral nerve cord of insects (Egger et al., 1997; Stephan et al., 2015), and nerve tracts of *C. elegans* (Chalfie and Thomson, 1979; Chalfie and Thomson, 1982). In these examples, MTs are distributed across the axonal profile; they are spaced from each other but appear only loosely cross-linked. Accordingly, conventional TEM strategies do not reveal conspicuous MT–MT connections as observed at the AIS. However, linkers clearly exist and become visible upon use of other strategies. For example, lanthanum is a trivalent cation that penetrates cell membranes if applied during fixation and severely enhances contrast of many subcellular structures upon TEM analysis (Leeson and Higgs, 1982; Shaklai and Tavassoli, 1982). In lanthanum-stained axons, MTs display irregular coating and fuzzy connections become visible between them (Burton and Fernandez, 1973; Lane and Treherne, 1970; Ochs and Burton, 1980). In classical freeze-etch preparations, nerves were detergent extracted, quick frozen, mechanically fractured to expose the inside, etched via freeze drying, and then rotary shadowed with platinum/carbon to produce a replica for analysis. Freeze-etch preparations clearly revealed 4- to 6-nm-thick MT–MT cross-bridges (Chen et al., 1992; Harada et al., 1994; Hirokawa, 1982, 1991).

Although nearest-neighbor MT–MT distances are not constant, their means show reproducible values that differ between neuron types and species (e.g., Fig. 4, A, F, and G); MTs are spaced on average ∼22 nm in parallel fibers of the mouse cerebellum (Chen et al., 1992), ∼110 nm in *Drosophila* (Egger et al., 1997; Stephan et al., 2015), and 9.8 nm in *C. elegans* (Krieg et al., 2017). In all of these cases, loss-of-function studies have revealed specific MAPs as MT–MT cross-linker candidates; loss of the *Drosophila* MAP1b homologue Futsch caused a reduction in nearest-neighbor values from ∼110 to ∼70 nm (Bettencourt da Cruz et al., 2005; Stephan et al., 2015), loss of ptl-1 (the *C. elegans* tau homologue) caused a reduction from 9.8 to 6.7 nm (Krieg et al., 2017), and loss of murine Mapt/tau abolished the majority of cross-bridges in freeze-etch preparations (Harada et al., 1994).

Differences in MT spacing become meaningful when comparing the longest isoforms of these three MAPs (all data taken from ensembl.org): ptl-1 (458 aa) is shorter than tau (749 aa),

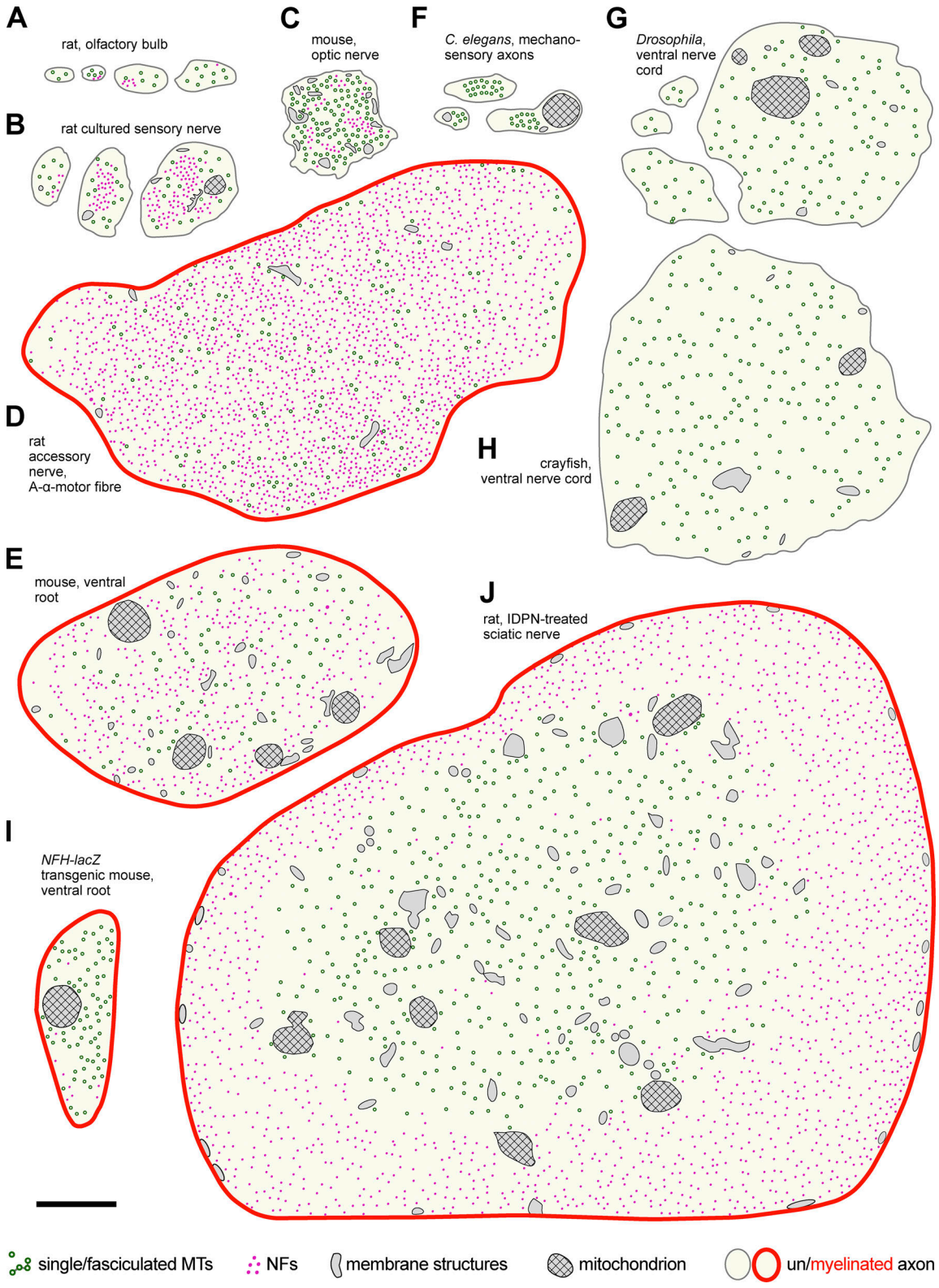

Figure 4. **MT and NF distributions in axon shafts of neurons in mammals, *C. elegans*, and arthropods.** Images represent axons in different animals, either wild type or genetically/pharmacologically manipulated, as indicated; they were drawn from Andres, 1965a (A); Bray and Bunge, 1981 (B); Nixon et al., 1994 (C); Zenker and Hohberg, 1973 (D); Eyer and Peterson, 1994 (E and I); Chalfie and Thomson, 1979 (F); Egger et al., 1997 (G); Ochs and Burton, 1980 (H); and Papasozomenos et al., 1981 (J). Best guesses were made with respect to structures shown. Abbreviations used: IDPN, β,β′-iminodipropionitrile; NFH-lacZ, lacZ knock-in into the heavy polypeptide NF gene. Scales in most original photos were given as magnifications (unfortunately meaningless in PDF format) and were estimated here by measuring MT diameters; suggested scale bar represents 500 nm throughout.

whereas Futsch is dramatically longer (5,495 aa). Futsch has a large repeat-rich central domain and its terminal regions show homology with the N- and C-terminal parts of human MAP1B, excluding however the two designated MT-binding domains (Fig. S1; Hummel et al., 2000; Villarroel-Campos and Gonzalez-Billault, 2014). It remains therefore to be seen whether Futsch achieves direct or indirect MT association through its terminal homology regions, which could mean that a single molecule could act as a MT–MT cross-linker.

In contrast, tau proteins binding to adjacent MTs were proposed to dimerize via their N-termini (Rosenberg et al., 2008), and the N-termini are clearly longer in tau (~450 aa) than in ptl-1 (~300 aa). A more recent model for tau-mediated MT–MT cross-linkage is less static and allows tau to diffuse (Méphon-Gaspard et al., 2016), consistent with observations that tau has a very short dwell time on MTs (Janning et al., 2014; Samsonov et al., 2004). Such loose binding dynamics might be one explanation for why MTs are not firmly interlinked into fascicles or hexagonal patterns but are free to detach and "diffuse" into empty areas of the axonal profile. This said, at high expression levels MAPs can very well induce hexagonal MT patterns (Chen et al., 1992), suggesting that MAP levels are well controlled in axons.

Surprisingly, the loss of specific MAPs (see above) did not cause a complete collapse of MTs onto each other. This may be explained by repulsion due to the high negative surface charge of MT lattices, but it more likely occurs through the expression of potentially redundant MAPs, as reviewed elsewhere (Bodakuntla et al., 2019; Burgoyne, 1991; Hahn et al., 2019; Hirokawa, 1991; Lee and Brandt, 1992; Matus, 1991). As a further complication, MAPs may change their affinities for MTs as a function of posttranslational tubulin modifications or tubulin isotypes. For example, polyglutamylation regulates binding of tau to MTs (Boucher et al., 1994). Furthermore, the average MT–MT distance of 9.8 nm in *C. elegans* (see above) was measured in mechanosensory neurons expressing mec-7 β-tubulin; upon mec7 deficiency, the same mechanosensory axons form MTs of smaller diameter, which display a reduced spacing of only 4 nm (Chalfie and Thomson, 1982; Krieg et al., 2017), suggesting that MTs with different tubulin isotypes are cross-linked differently.

In arthropods, the shafts of small- and large-caliber axons form identical MT networks

The organizational principle described for small-caliber axons appears to be maintained in large-diameter axons of crustaceans, insects, or spiders; MTs are distributed across the axon profile and, where data are given, nearest-neighbor distances are typically 100–200 nm (Fig. 4, G and H; Bettencourt da Cruz et al., 2005; Burton and Fernandez, 1973; Egger et al., 1997; Foelix and Hebets, 2001; Foelix and Troyer, 1980; King and Wyman, 1980; Lane and Abbott, 1975; Nadelhaft, 1974; Smith et al., 1977; Stephan et al., 2015; Viancour et al., 1987; Warren, 1984).

In crustaceans, lanthanum staining revealed "axoplasmic matrix proteins" in the form of 5- to 10-nm-thick MT–MT cross-bridges (Burton and Fernandez, 1973; Ochs and Burton, 1980). Upon extraction with glycerol-sucrose-DMSO solution, MT–MT distances were seen to collapse, and the extracted protein was of high weight and heat stable, as is typical of MAPs (Warren, 1984). An anti-NF antibody (clone NN18) stained the cross-bridges and detected a 600-kD protein with homology to MAP1B (Weaver and Viancour, 1991; Weaver and Viancour, 1992; but see Corrêa et al., 2004).

These data match very well with those for the *Drosophila* Futsch protein: like observed in crustaceans, Futsch spaces MTs at ~110 nm (see above; Stephan et al., 2015), displays MAP1B homology, and its central domain is composed of 60 repeats with intermediate filament homology (Hummel et al., 2000). In support of this notion, arthropod genomes, including crayfish (asterisk in Fig. S2), tend to contain Futsch-like genes, which display homology with Futsch in exactly those N- and C-terminal regions that are also homologous to human MAP1B (Fig. S1).

In addition to MT–MT linkers, also cross-bridges from MTs to the cortex were reported in crayfish (Burton and Fernandez, 1973). Extrapolating from work in *Drosophila*, these might be large ankyrins (Anks). Thus, long isoforms of cortex-associated Ank2 join forces with Futsch to form MT–MT networks that help to expand and maintain axon calibers in *Drosophila* (Stephan et al., 2015). Also in *C. elegans*, large Anks seem to anchor MTs along the axon shaft (He et al., 2020), and large AnkB isoforms appear to perform similar functions along axon shafts in mouse (Yang et al., 2019), consistent with reports of ~100-nm-long filaments linking the plasmalemma to MTs in freeze-etch preparations of frog axons (Hirokawa, 1982). For a discussion of further candidate factors involved in surface anchorage of MTs, see Hahn et al. (2019).

Taken together, different arthropod species seem to use a consistent strategy of MT cross-linkage across a wide range of axon diameters (~0.1 to ~60 µm). Although Futsch-like proteins seem the most prominent players, further MAPs such as Tau or Ensconsin, or even type 6 kinesins, might contribute to these networks (Hahn et al., 2016; Monroy et al., 2018).

In vertebrates, NFs contribute to caliber enlargement of axons

A major difference between axons of arthropods and vertebrates is the presence of NFs. Cytoplasmic intermediate filaments are clearly absent in arthropods (Peter and Stick, 2015), whereas NFs are highly abundant in large-caliber axons of vertebrates where they are spaced out and distributed in a similar manner as described for MTs (details below; Fig. 4, D and E; Hirokawa, 1991; Peters et al., 1991).

NFs of vertebrates are ~10 nm thick, highly stretch-resistant intermediate filaments composed of a chain of hetero-oligomeric subunits (Fig. S2). Each subunit contains a mix of type IV proteins encoded by different genes (Fig. S2 A; Herrmann and Aebi, 2016; Kornreich et al., 2015; Perrot et al., 2008), usually including a lightweight (α-internexin, 66 kD; or NF-L, 62 kD), medium-weight (NF-M, 103 kD), and heavyweight (NF-H, 117 kD) protein, from now referred to as α, L, M, and H. These proteins can coassemble with type III peripherin (Yuan et al., 2012). In small unmyelinated fibers, peripherin even seems to be the predominant NF component (Larivière et al., 2002). However, in large myelinated fibers, neither loss nor gain of

peripherin has revealed major impacts on NF formation, although long-term overexpression triggers amyotrophic lateral sclerosis–like axonopathy (Beaulieu et al., 1999; Larivière et al., 2002).

NFs promote large axon diameters, as is clearly demonstrated by axon-caliber reduction in NF-deficient mouse and quail models or human patients (Eyer and Peterson, 1994; Sakaguchi et al., 1993; Yamasaki et al., 1991; Yum et al., 2009). H, M, L, and α seem to contribute to different degrees; calibers of large axons were strongly reduced and NFs virtually absent in $L^{-/-}$ mutant mice, quail, and humans, whereas both parameters were only moderately affected in $M^{-/-}$ and marginally in $H^{-/-}$ and $\alpha^{-/-}$ mutant mice (Beaulieu et al., 1999; Elder et al., 1998; Jacomy et al., 1999; Levavasseur et al., 1999; Ohara et al., 1993; Yamasaki et al., 1992; Yum et al., 2009; Zhu et al., 1997, 1998). However, masked redundant roles of H and α became apparent in $H^{-/-}$ $M^{-/-}$ or $\alpha^{-/-}$ $L^{-/-}$ double-mutant mice, which displayed complete or next to complete NF depletion (Jacomy et al., 1999; Levavasseur et al., 1999). Importantly, NF proteins have to be present in proportional amounts. Overexpression of M or H (but not L) caused axon-caliber reduction, which was even further enhanced upon MH coexpression; in contrast, LM or LH coexpressions caused caliber increases (Xu et al., 1996).

Caliber enlargement can also be achieved by applying the neurotoxin β,β'-iminodipropionitrile: in treated axons, proximal segments enlarge due to NF accumulation; this crowding of filaments does not affect NF-NF spacing (39–46 nm; Parhad et al., 1987), suggesting that NF networks have the physical ability to drive axon enlargement. Comparable NF-driven axon caliber expansions are also observed during giant axonal neuropathy, primarily in internode regions of myelinated fibers (Asbury et al., 1972; Berg et al., 1972).

NF–NF spacing depends on the tail domains of NF proteins (Fig. S2). The tail domains differ in lengths (H, 679 aa; M, 514 aa; L, 158 aa; and α, 91 aa) and stick out from NFs like the hairs on a pipe brush (Fig. S2; Kornreich et al., 2015; Stevens and Hoh, 2010). Freeze-etch analyses of axons revealed 20- to 60-nm-long and 4- to 6-nm-thick NF–NF cross-bridges with a periodicity of 20–100 nm and containing at least the tail domain of H (Hirokawa, 1982; Hirokawa et al., 1984; Schnapp and Reese, 1982). TEM analyses confirmed the existence of ∼45-nm-long cross-bridges in myelinated axons, whereas they only measured ∼30 nm at the NoR or in dendrites, which both lack myelin (Hsieh et al., 1994; Wuerker and Palay, 1969). A very similar reduction to 30 nm was observed in myelinated axons lacking the myelin component myelin-associated glycoprotein (Yin et al., 1998). This led to the hypothesis that myelin-associated glycoprotein–dependent phosphorylation of M/H tails (Fig. S2) at their ∼7/∼51 KSP motifs triggers cross-bridge extension, hence the increased NF spacing in myelinated axons (Nixon et al., 1994; Garcia et al., 2003; Kumar and Hoh, 2004 and references therein).

Consistent with the knockout data, systematic tail domain deletions ($^{tail\Delta}$) in transgenic mice revealed a reduction in cross-bridge numbers in axons of $H^{tail\Delta}$ or $M^{tail\Delta}$ mutant mice, but only for $M^{tail\Delta}$ did this result in narrower axons and slightly shorter NF spacing (39 nm); in $M^{tail\Delta}$ $H^{tail\Delta}$ double-mutant mice NF–NF side bridges were absent and axon diameters were further reduced (Garcia et al., 2003; Rao et al., 2002), lending further support to the idea of redundancy between M and H. Surprisingly, $M^{tail\Delta}$ $H^{tail\Delta}$ filaments still ran in parallel to the axon axis and maintained a spacing of ∼30 nm, likely mediated by the shorter tail domains of L and/or α (Kornreich et al., 2015). Consistent with these findings, application of osmotic shock induced by high sucrose in axons or polyethylene glycol in vitro (likely abolishing charge-dependent extensions in particular of H and M tails), caused a severe reduction in NF spacing, but not a total collapse (Friede and Samorajski, 1970; Kornreich et al., 2015).

Therefore, in contrast to modular MT–MT coupling, which depends on separately encoded MAPs, NF–NF linkage and spacing is a function of the filaments themselves and can be regulated through phosphorylation. It appears that their cross-linking affinities are low enough so that NF–NF networks can undergo dynamic changes, as was similarly discussed for MT–MT networks.

In large-caliber axon shafts of vertebrates, MTs intermingle with NFs

NFs tend to be sparse in small axons. However, with increasing diameters, NF numbers rise dramatically (much faster than MT numbers) and may eventually outnumber MTs by an order of magnitude (Table S2; Fig. 4, A–E; Alfei et al., 1991; Alvarez et al., 1982; Malbouisson et al., 1985; Pannese et al., 1981). This trend applies to myelinated and unmyelinated axons (Friede and Samorajski, 1970; Smith et al., 1970), although some exceptional reports find constant MT densities across different caliber ranges (Elder et al., 1998; Zenker and Hohberg, 1973), and NF/MT ratios in the extraordinarily large giant axons of squid seem to be as low as 2:1 (Fath and Lasek, 1988). However, in general, MT densities in large-caliber axons of vertebrates tend to be lower than in arthropods due to the presence/absence of NFs; for example, MT densities in axons of lamprey are approximately an eighth compared with densities in cockroach axons of similar diameter (Table S2).

Images and descriptions of small versus large caliber axons across vertebrate species suggest fundamental differences in MT distribution (Nakazawa and Ishikawa, 1995; Peters et al., 1991; Raine et al., 1971; Tanner et al., 1998; Tsukita and Ishikawa, 1981; and references listed in Table S2). In small fibers (Fig. 4, A–C), MT–MT and NF–NF networks tend to segregate, which may be a function of their composition (e.g., predominance of peripherin; see above) and/or of their numbers. With increasing NF numbers, there is a clear impact on MT organization (Fig. 4, D and E) in that patches of MT–MT networks become rarer and smaller, and often single MTs seem to "dissolve" into the surrounding "sea" of NF–NF networks, thus spreading out at low densities across axonal profiles.

To act as a "solvent," NFs would have to be able to cross-link to MTs, and this seems to be the case: in nonneuronal cells, the cell-junctional scaffold protein plectin was described as a cross-linker between MTs and the intermediate filament vimentin (Svitkina et al., 1996); in axons, MT–NF cross-bridges have also been described (Hirokawa, 1991; Rice et al., 1980; Schnapp and

Reese, 1982). Such cross-bridges were suggested to be MAPs or MAP-like factors (e.g., tau, MAP2, or MAP6) or even motor proteins (Leterrier et al., 1982; Miyata et al., 1986; Perrot et al., 2008). Unlike the regular side-arms of NFs, MT–NF linkers in axons were described to display random periodicity, and their shapes were often bifurcating with a length of 54.7 nm, which was distinct from the spacing of MT–MT (49.6 nm) or NF–NF (40.61 nm) cross-bridges (Monaco et al., 1989; Tsukita et al., 1982).

NFs are proposed to form "hydrogel networks" (Kornreich et al., 2015) and to behave like "inert 'molecules' in a dilute solution" that "are relatively free to move apart from each other and to fill the available space within the axon" (Price et al., 1988). This would mean that also MTs dissolved in these networks are fairly free to drift, ideal to accommodate dynamic space requirements, for example when voluminous cargoes are transported through an axonal region. In support of this idea, serial TEM analyses of axons reveal loose parallel arrangements, with MTs changing their relative positions in consecutive axon segments (Fig. 1 A; Bray and Bunge, 1981; Tsukita and Ishikawa, 1981). Furthermore, MTs often cluster around mitochondria (Friede and Samorajski, 1970; Hirokawa, 1982; Malbouisson et al., 1985; Pannese et al., 1981; Raine et al., 1971; Smith et al., 1975, 1977; Tsukita and Ishikawa, 1981). This suggests that MTs can be attracted toward mitochondria, likely mediated by MT–mitochondrial linkers that have a higher affinity than MT–MT or MT–NF linkers. These could be MT-associated motor protein complexes for mitochondria that are being transported (Hirokawa et al., 2010) or the cross-linker protein syntaphilin known to dock or anchor stationary mitochondria to MTs (Kang et al., 2008; Lin et al., 2017). The same logic may apply to occasional groups of narrowly cross-bridged MT fascicles positioned within NF-rich axon shafts of lamprey neurons (Smith et al., 1970, 1975).

In the absence of NFs, MTs form functional structural networks

Surprisingly, removal of the highly abundant NF–NF networks from axons is not a lethal condition, although up to 20% of axons can be lost, and axon calibers and their conduction velocities are significantly reduced (Beaulieu et al., 1999; Bocquet et al., 2009; Eyer and Peterson, 1994; Jacomy et al., 1999; Križ et al., 2000; Sakaguchi et al., 1993; Yamasaki et al., 1991; Yum et al., 2009; Zhu et al., 1997). In the absence of NFs, the densities of MTs increase up to 10-fold, but they are well organized and look very similar to those of small-caliber vertebrate axons or axons of arthropod neurons; MTs are distributed across the axonal profile and seem to maintain an average nearest-neighbor spacing from each other (Fig. 4 I versus Fig. 4, A–C and F–H).

In lower motorneurons of rat, MAPs localize to MTs scattered throughout the axonal profile (Papasozomenos et al., 1985). This suggests that the typical MT-regulating machinery is readily available so that MTs can interact in meaningful ways even when dissolved into NF–NF networks. Such a scenario could explain why loss of function of the MT-binding and -regulating spectraplakin dystonin causes severe disorganization of axonal MTs regardless of whether NFs are present or absent (Bernier and Kothary, 1998; Dalpe et al., 1998; Eyer et al., 1998; Voelzmann et al., 2017) and that even loss of its fly homologue Short stop causes the same phenotype (Alves-Silva et al., 2012; Sánchez-Soriano et al., 2009).

This said, NF depletion might impact on MTs. For example, NFs were reported to regulate MT stability and/or polymerization (Bocquet et al., 2009; Kurup et al., 2018 and references therein). This might explain why the number of MTs per axon was doubled in $H^{-/-}$ single-mutant mice, although NF numbers and axon diameters were hardly affected in these animals (Jacomy et al., 1999; Zhu et al., 1998). In contrast, there seems to be no up-regulation of MT numbers in NF-depleted *quiver* mutant quail axons when calculating increases in MT density against the reduction in cross-sectional area (Yamasaki et al., 1991).

Regardless of whether MT numbers change, NF-depletion provides unique opportunities to study the "default" MT–MT networks in large caliber axons. For example, nearest-neighbor relationships of MTs are impossible to assess in larger axons where MTs are dissolved into NF–NF networks. Depletion of NFs would therefore provide a condition where true spacing could be assessed, thus providing improved strategies to study MAP functions in these neurons.

An efficient experimental strategy to generate NF-free MT–MT networks is provided by the injection of the toxins 2,5-hexanedione or β,β'-iminodipropionitrile. Apart from affecting the proximodistal NF distribution in axons (see above), these toxins trigger a dramatic segregation of the axonal cytoskeleton: within hours or days, a core of MT–MT networks forms, surrounded by a halo of NF–NF networks (Fig. 4 J; Griffin et al., 1983a, 1983b; Papasozomenos et al., 1981; Parhad et al., 1987). Importantly, the central MT–MT networks were shown to form MAP1A/B immunoreactive cross-bridges in sciatic nerve (Hirokawa et al., 1985) and overlap with MAP staining in the ventral root (Papasozomenos et al., 1985), suggesting that MTs brought their MT-regulating machinery into this core when segregating away from NFs.

The underlying mechanisms of this segregation process remain hypothetical. A mathematical model has been proposed stating that cytoskeletal segregation is caused by a reduction in slow MT-based transport of NFs, thus shifting the bias toward other transported cargoes that may cross-link MTs and zip them together (Xue et al., 2015). Similar mechanisms might explain comparable segregations that occur in a number of axonal pathologies, although with certain variations; for example, in giant axonal neuropathy, MT–MT networks form not at the core but in the axon periphery (Asbury et al., 1972; Berg et al., 1972; further references in Xue et al., 2015).

Conclusions and final remarks

This review aimed to understand concepts of axonal architecture by integrating knowledge from >50 yr of study across a range of animal models, including arthropods that have developed their axonal organization in the absence of NFs. From this, I propose that loose MT–MT networks are a fundamental common element of axons. In these networks, MTs are spaced out and only loosely connected by MAPs, thus allowing for flexible

rearrangement, for example to permit and support the passing through of large transported cargoes. The main exception to this rule are fasciculated MTs at the AIS or in stem axons where tight coupling might represent a structural feature to resist the mechanical forces caused by a tug-of-war between antagonistic motor activities.

As discussed elsewhere (Hahn et al., 2019), essential architectural properties of axons depend on stable MTs and a stiff cortex. In contrast, the addition of NF–NF networks appears to have its major purpose in expanding axon calibers, thus improving conduction velocity and spike frequency (Friede et al., 1984; Perge et al., 2009, 2012). However, NFs seem to make astonishingly little contribution to axonal integrity and sustainability. NFs might improve elastic properties of axons, but arthropods clearly demonstrate that caliber enlargements can be achieved solely through increased MT numbers. In large-caliber axons of arthropods, most MTs seem to serve a mere structural purpose, with only a specialized subset used for axonal transport (Miller et al., 1987). This might explain why it was possible during evolution to replace a fraction of the axonal MTs by NFs in other animal groups.

If MT networks are indeed the key element of the longitudinal axonal cytoskeleton, it makes sense that MT-regulating mechanisms are functional in small- and large-caliber axons of vertebrates alike. Accordingly, MTs seem to be equipped with their regulatory toolbox even when submerged into the vast NF–NF networks, enabling them to interact in meaningful ways and to rapidly form intact MT–MT networks when cytoskeletal segregation occurs after 2,5-hexanedione or β,β′-iminodipropionitrile application.

I hope that the descriptions throughout this review have made clear how much information and understanding can be obtained from the retrospective study of classical EM work, which has become easily accessible thanks to the efforts of most journals to systematically digitize their back issues. There is wealth of information for many other contemporary lines of investigation, such as detailed descriptions of MT behaviors during axon branching (Yu et al., 1994), of the ultrastructure of growth cones, dendrites, and synapses (Peters et al., 1991), or of curious phenomena such as impressive packages of ER-derived tubular structures found in certain axons (Andres, 1965b; Peters et al., 1991). Axonal MTs of species as diverse as cockroach, lamprey, frog, toad, chick, mouse, and rats were reported to contain luminal material in form of a ∼4-nm-thick central dot or filament (Andres, 1965a; Burton, 1984, 1987; Gonatas and Robbins, 1965; Lane and Treherne, 1970; Nixon et al., 1994; Rodríguez Echandía et al., 1968; Smith et al., 1970, 1975; Wuerker and Palay, 1969), matching recent reports of MTs with incorporated actin filaments or MAP6/stable tubule-only peptide (Cuveillier et al., 2020; Paul et al., 2019 *Preprint*), of which the latter could help to explain long-term cold resistance of axonal MTs observed in vivo (Delphin et al., 2012; Pannese et al., 1982; but see also Song et al., 2013). Furthermore, classical studies revealed the presence of post-translationally modified subdomains in MT lattices (Baas and Ahmad, 1992; Baas and Black, 1990; Baas and Joshi, 1992), which start finding their explanations in current models of MT stability (Baas et al., 2016).

In conclusion, I hope that this review will help to build bridges to the past to capitalize on that valuable treasure trove that can complement and often even instruct our work with modern techniques in meaningful ways. But it should also have become clear that existing descriptions only scratch the surface of what we need to understand. Classical EM techniques had clear limitations with respect to efficiency and the use of fixation and staining methods that might not always represent axonal structure in all accuracy. New techniques such as large-volume EM or cryo-electron tomography (Kubota et al., 2018; Xu et al., 2017; Chakraborty et al., 2020) provide ever-improving means to drive the discovery processes toward good understanding of axon structure, which will eventually have important implications for work on neuronal pathologies.

Online supplemental material

Fig. S1 shows the homology of *Drosophila* Futsch to human MAP1B and Futsch-like genes in other invertebrates. Fig. S2 shows the composition of NFs. Table S1 contains ultrastructural reports of AISs in different neuron types. Table S2 contains axonal MT and NF numbers as reported in the literature.

Acknowledgments

The author is most grateful to Christophe Leterrier and Anthony Brown for constructive feedback and most valuable comments and advice; Yanhe Li for sharing the genomic sequence of crayfish; and Llilians Calvo-González for extracting fragments homologous to Futsch; Paul Conduit, Matthew Ronshaugen, and Andre Voelzmann for feedback; Samuel Shields for kind support with literature searches; and the Manchester University Library for their outstanding services.

Work underpinning this article was made possible through support by the Biotechnology and Biological Sciences Research Council to A. Prokop (grants BB/I002448/1, BB/P020151/1, BB/L000717/1, and BB/M007553/1).

The author declares no competing financial interests.

Submitted: 18 December 2019
Revised: 13 April 2020
Accepted: 14 April 2020

References

Akin, E.J., L. Solé, S.D. Dib-Hajj, S.G. Waxman, and M.M. Tamkun. 2015. Preferential targeting of Nav1.6 voltage-gated Na^+ Channels to the axon initial segment during development. *PLoS One*. 10. e0124397. https://doi.org/10.1371/journal.pone.0124397

Al-Bassam, S., M. Xu, T.J. Wandless, and D.B. Arnold. 2012. Differential trafficking of transport vesicles contributes to the localization of dendritic proteins. *Cell Reports*. 2:89–100. https://doi.org/10.1016/j.celrep.2012.05.018

Albrecht, D., C.M. Winterflood, M. Sadeghi, T. Tschager, F. Noé, and H. Ewers. 2016. Nanoscopic compartmentalization of membrane protein motion at the axon initial segment. *J. Cell Biol.* 215:37–46. https://doi.org/10.1083/jcb.201603108

Alfei, L., L. Medolago Albani, A.R. Mosetti, C. Scarfo, and A. Stefanelli. 1991. Cytoskeletal components and calibers in developing fish Mauthner axon (*Salmo gairdneri* Rich.). *J. Comp. Neurol.* 314:164–170. https://doi.org/10.1002/cne.903140115

Altschul, S.F., T.L. Madden, A.A. Schäffer, J. Zhang, Z. Zhang, W. Miller, and D.J. Lipman. 1997. Gapped BLAST and PSI-BLAST: a new generation of protein database search programs. *Nucleic Acids Res.* 25:3389–3402. https://doi.org/10.1093/nar/25.17.3389

Alvarez, J., F. Arredondo, F. Espejo, and V. Williams. 1982. Regulation of axonal microtubules: effect of sympathetic hyperactivity elicited by reserpine. *Neuroscience*. 7:2551–2559. https://doi.org/10.1016/0306-4522(82)90214-7

Alves-Silva, J., N. Sánchez-Soriano, R. Beaven, M. Klein, J. Parkin, T.H. Millard, H.J. Bellen, K.J.T. Venken, C. Ballestrem, R.A. Kammerer, et al. 2012. Spectraplakins promote microtubule-mediated axonal growth by functioning as structural microtubule-associated proteins and EB1-dependent +TIPs (tip interacting proteins). *J. Neurosci.* 32:9143–9158. https://doi.org/10.1523/JNEUROSCI.0416-12.2012

Andres, K.H. 1965a. Der Feinbau des Bulbus olfactorius der Ratte unter besonderer Berücksichtigung der synaptischen Verbindungen. *Z Zellforsch.* 65:530–561. https://doi.org/10.1007/BF00337067

Andres, K.H. 1965b. Über die Feinstruktur besonderer Einrichtungen in markhaltigen Nervenfasern des Kleinhirns der Ratte. *Z. Zellforsch. Mikrosk. Anat.* 65:701–712. https://doi.org/10.1007/BF00342591

Ango, F., G. di Cristo, H. Higashiyama, V. Bennett, P. Wu, and Z.J. Huang. 2004. Ankyrin-based subcellular gradient of neurofascin, an immunoglobulin family protein, directs GABAergic innervation at purkinje axon initial segment. *Cell*. 119:257–272. https://doi.org/10.1016/j.cell.2004.10.004

Asbury, A.K., M.K. Gale, S.C. Cox, J.R. Baringer, and B.O. Berg. 1972. Giant axonal neuropathy--a unique case with segmental neurofilamentous masses. *Acta Neuropathol.* 20:237–247. https://doi.org/10.1007/BF00686905

Baas, P.W.. 2002. Microtubule transport in the axon. *Int. Rev. Cytol.* 212:41–62. https://doi.org/10.1016/S0074-7696(01)12003-6

Baas, P.W., and F.J. Ahmad. 1992. The plus ends of stable microtubules are the exclusive nucleating structures for microtubules in the axon. *J. Cell Biol.* 116:1231–1241. https://doi.org/10.1083/jcb.116.5.1231

Baas, P.W., and M.M. Black. 1990. Individual microtubules in the axon consist of domains that differ in both composition and stability. *J. Cell Biol.* 111:495–509. https://doi.org/10.1083/jcb.111.2.495

Baas, P.W., J.S. Deitch, M.M. Black, and G.A. Banker. 1988. Polarity orientation of microtubules in hippocampal neurons: uniformity in the axon and nonuniformity in the dendrite. *Proc. Natl. Acad. Sci. USA.* 85:8335–8339. https://doi.org/10.1073/pnas.85.21.8335

Baas, P.W., and H.C. Joshi. 1992. Gamma-tubulin distribution in the neuron: implications for the origins of neuritic microtubules. *J. Cell Biol.* 119:171–178. https://doi.org/10.1083/jcb.119.1.171

Baas, P.W., and S. Lin. 2011. Hooks and comets: The story of microtubule polarity orientation in the neuron. *Dev. Neurobiol.* 71:403–418. https://doi.org/10.1002/dneu.20818

Baas, P.W., A.N. Rao, A.J. Matamoros, and L. Leo. 2016. Stability properties of neuronal microtubules. *Cytoskeleton (Hoboken)*. 73:442–460. https://doi.org/10.1002/cm.21286

Baas, P.W., C. Vidya Nadar, and K.A. Myers. 2006. Axonal transport of microtubules: the long and short of it. *Traffic*. 7:490–498. https://doi.org/10.1111/j.1600-0854.2006.00392.x

Balasanyan, V., K. Watanabe, W.P. Dempsey, T.L. Lewis, Jr., L.A. Trinh, and D.B. Arnold. 2017. Structure and function of an actin-based filter in the proximal axon. *Cell Reports*. 21:2696–2705. https://doi.org/10.1016/j.celrep.2017.11.046

Beaulieu, J.M., M.D. Nguyen, and J.P. Julien. 1999. Late onset of motor neurons in mice overexpressing wild-type peripherin. *J. Cell Biol.* 147:531–544. https://doi.org/10.1083/jcb.147.3.531

Berg, B.O., S.H. Rosenberg, and A.K. Asbury. 1972. Giant axonal neuropathy. *Pediatrics*. 49:894–899.

Berger, S.L., A. Leo-Macias, S. Yuen, L. Khatri, S. Pfennig, Y. Zhang, E. Agullo-Pascual, G. Caillol, M.S. Zhu, E. Rothenberg, et al. 2018. Localized myosin II activity regulates assembly and plasticity of the axon initial segment. *Neuron*. 97:555–570.

Bernier, G., and R. Kothary. 1998. Prenatal onset of axonopathy in Dystonia musculorum mice. *Dev. Genet.* 22:160–168. https://doi.org/10.1002/(SICI)1520-6408(1998)22:2<160::AID-DVG5>3.0.CO;2-4

Bettencourt da Cruz, A., M. Schwärzel, S. Schulze, M. Niyyati, M. Heisenberg, and D. Kretzschmar. 2005. Disruption of the MAP1B-related protein FUTSCH leads to changes in the neuronal cytoskeleton, axonal transport defects, and progressive neurodegeneration in *Drosophila*. *Mol. Biol. Cell*. 16:2433–2442. https://doi.org/10.1091/mbc.e04-11-1004

Bird, M.M., and A.R. Lieberman. 1976. Microtubule fascicles in the stem processes of cultured sensory ganglion cells. *Cell Tissue Res.* 169:41–47. https://doi.org/10.1007/BF00219306

Bocquet, A., R. Berges, R. Frank, P. Robert, A.C. Peterson, and J. Eyer. 2009. Neurofilaments bind tubulin and modulate its polymerization. *J. Neurosci.* 29:11043–11054. https://doi.org/10.1523/JNEUROSCI.1924-09.2009

Bodakuntla, S., A.S. Jijumon, C. Villablanca, C. Gonzalez-Billault, and C. Janke. 2019. Microtubule-Associated Proteins: Structuring the Cytoskeleton. *Trends Cell Biol.* 29:804–819. https://doi.org/10.1016/j.tcb.2019.07.004

Bolós, M., J. Terreros-Roncal, J.R. Perea, N. Pallas-Bazarra, J. Ávila, and M. Llorens-Martín. 2019. Maturation dynamics of the axon initial segment (AIS) of newborn dentate granule cells in young adult C57BL/6J mice. *J. Neurosci.* 39:1605–1620.

Boucher, D., J.C. Larcher, F. Gros, and P. Denoulet. 1994. Polyglutamylation of tubulin as a progressive regulator of in vitro interactions between the microtubule-associated protein Tau and tubulin. *Biochemistry*. 33:12471–12477. https://doi.org/10.1021/bi00207a014

Bray, D., and M.B. Bunge. 1981. Serial analysis of microtubules in cultured rat sensory axons. *J. Neurocytol.* 10:589–605. https://doi.org/10.1007/BF01262592

Brown, A., and R.J. Lasek. 1990. The Cytoskeleton of the Squid Giant Axon. *In* Squid as Experimental Animals. D.L. Gilbert, W.J. Adelman, and J.M. Arnold, editors. Springer US, Boston. pp. 235–302. https://doi.org/10.1007/978-1-4899-2489-6_14

Burgoyne, R.D. 1991. High molecular weight microtubule-associated proteins of brain. *In* The Neuronal Cytoskeleton. R. Burgoyne, editor. Wiley-Liss, New York. 75–91.

Burrows, M. 1996. The Neurobiology of an Insect Brain. Oxford University Press, New York. 682 pp. https://doi.org/10.1093/acprof:oso/9780198523444.001.0001

Burton, P.R.. 1984. Luminal material in microtubules of frog olfactory axons: structure and distribution. *J. Cell Biol.* 99:520–528. https://doi.org/10.1083/jcb.99.2.520

Burton, P.R.. 1987. Microtubules of frog olfactory axons: their length and number/axon. *Brain Res.* 409:71–78. https://doi.org/10.1016/0006-8993(87)90742-6

Burton, P.R., and H.L. Fernandez. 1973. Delineation by lanthanum staining of filamentous elements associated with the surfaces of axonal microtubules. *J. Cell Sci.* 12:567–583.

Burton, P.R., and L.A. Laveri. 1985. The distribution, relationships to other organelles, and calcium-sequestering ability of smooth endoplasmic reticulum in frog olfactory axons. *J. Neurosci.* 5:3047–3060. https://doi.org/10.1523/JNEUROSCI.05-11-03047.1985

Calkins, D.J. 2013. Age-Related Changes in the Visual Pathways: Blame It on the AxonAge-Related Changes in the Visual Pathways. *Invest. Ophthalmol. Vis. Sci.* 54:ORSF 37–41.

Castel, M., M.E. Spira, I. Parnas, and Y. Yarom. 1976. Ultrastructure of region of a low safety factor in inhomogeneous giant axon of the cockroach. *J. Neurophysiol.* 39:900–908. https://doi.org/10.1152/jn.1976.39.4.900

Chakraborty, S., M. Jasnin, and W. Baumeister. 2020. Three-dimensional organization of the cytoskeleton: a cryo-electron tomography perspective. *Protein Sci.* https://doi.org/10.1002/pro.3858

Chalfie, M., and J.N. Thomson. 1979. Organization of neuronal microtubules in the nematode Caenorhabditis elegans. *J. Cell Biol.* 82:278–289. https://doi.org/10.1083/jcb.82.1.278

Chalfie, M., and J.N. Thomson. 1982. Structural and functional diversity in the neuronal microtubules of Caenorhabditis elegans. *J. Cell Biol.* 93:15–23. https://doi.org/10.1083/jcb.93.1.15

Chan-Palay, V.. 1972. The tripartite structure of the undercoat in initial segments of Purkinje cell axons. *Z. Anat. Entwicklungsgesch.* 139:1–10. https://doi.org/10.1007/BF00519921

Chen, J., Y. Kanai, N.J. Cowan, and N. Hirokawa. 1992. Projection domains of MAP2 and tau determine spacings between microtubules in dendrites and axons. *Nature*. 360:674–677. https://doi.org/10.1038/360674a0

Cohen, M.J. 1967. Correlation between structure, function and RNA metabolism in central neurons of insects. *In* Invertebrate Nervous Systems: Their Significance for Mammalian Neurophysiology. Vol. 1. C.A.G. Wiersma, editor. The University of Chicago Press, Chicago. 65–78.

Conradi, S.. 1969. Observations on the ultrastructure of the axon hillock and initial axon segment of lumbosacral motoneurons in the cat. *Acta Physiol. Scand. Suppl.* 332:65–84.

Conradi, S., and S. Skoglund. 1969. Observations on the ultrastructure of the initial motor axon segment and dorsal root boutons on the motoneurons in the lumbosacral spinal cord of the cat during postnatal development. *Acta Physiol. Scand. Suppl.* 333:53–76.

Corrêa, C.L., S.F. da Silva, J. Lowe, G.G. Tortelote, M. Einicker-Lamas, A.M. Martinez, and S. Allodi. 2004. Identification of a neurofilament-like

protein in the protocerebral tract of the crab *Ucides cordatus*. *Cell Tissue Res*. 318:609–615. https://doi.org/10.1007/s00441-004-0992-5

Costa, A.R., R. Pinto-Costa, S.C. Sousa, and M.M. Sousa. 2018. The regulation of axon diameter: from axonal circumferential contractility to activity-dependent axon swelling. *Front. Mol. Neurosci*. 11:319. https://doi.org/10.3389/fnmol.2018.00319

Costa, A.R., S.C. Sousa, R. Pinto-Costa, J.C. Mateus, C.D.F. Lopes, A.C. Costa, D. Rosa, D. Machado, L. Pajuelo, X. Wang, et al. 2020. The membrane periodic skeleton is an actomyosin network that regulates axonal diameter and conduction. *eLife*. 9. e55471. https://doi.org/10.7554/eLife.55471

Cunha-Ferreira, I., A. Chazeau, R.R. Buijs, R. Stucchi, L. Will, X. Pan, Y. Adolfs, C. van der Meer, J.C. Wolthuis, O.I. Kahn, et al. 2018. The HAUS complex is a key regulator of non-centrosomal microtubule organization during neuronal development. *Cell Reports*. 24:791–800. https://doi.org/10.1016/j.celrep.2018.06.093

Cuveillier, C., J. Delaroche, M. Seggio, S. Gory-Fauré, C. Bosc, E. Denarier, M. Bacia, G. Schoehn, H. Mohrbach, I. Kulić, A. Andrieux, I. Arnal, and C. Delphin. 2020. MAP6 is an intraluminal protein that induces neuronal microtubules to coil. *Sci. Adv*. 6:eaaz4344.

Dalpe, G., N. Leclerc, A. Vallee, A. Messer, M. Mathieu, Y. De Repentigny, and R. Kothary. 1998. Dystonin is essential for maintaining neuronal cytoskeleton organization. *Mol. Cell. Neurosci*. 10:243–257. https://doi.org/10.1006/mcne.1997.0660

de Zeeuw, C.I., T.J.H. Ruigrok, J.C. Holstege, M.P.A. Schalekamp, and J. Voogd. 1990. Intracellular labeling of neurons in the medial accessory olive of the cat: III. Ultrastructure of axon hillock and initial segment and their GABAergic innervation. *J. Comp. Neurol*. 300:495–510. https://doi.org/10.1002/cne.903000405

Deller, T., M. Korte, S. Chabanis, A. Drakew, H. Schwegler, G.G. Stefani, A. Zuniga, K. Schwarz, T. Bonhoeffer, R. Zeller, et al. 2003. Synaptopodin-deficient mice lack a spine apparatus and show deficits in synaptic plasticity. *Proc. Natl. Acad. Sci. USA*. 100:10494–10499. https://doi.org/10.1073/pnas.1832384100

Delphin, C., D. Bouvier, M. Seggio, E. Couriol, Y. Saoudi, E. Denarier, C. Bosc, O. Valiron, M. Bisbal, I. Arnal, et al. 2012. MAP6-F is a temperature sensor that directly binds to and protects microtubules from cold-induced depolymerization. *J. Biol. Chem*. 287:35127–35138. https://doi.org/10.1074/jbc.M112.398339

Dubey, S., N. Bhembre, S. Bodas, S. Veer, A. Ghose, A. Callan-Jones, and P. Pullarkat. 2020. The axonal actin-spectrin lattice acts as a tension buffering shock absorber. *eLife*. 9. https://doi.org/10.7554/eLife.51772

Dzhashiashvili, Y., Y. Zhang, J. Galinska, I. Lam, M. Grumet, and J.L. Salzer. 2007. Nodes of Ranvier and axon initial segments are ankyrin G–dependent domains that assemble by distinct mechanisms. *Journal of Cell Biology*. 177(5):857–870.

Egger, M.D., R.S. Nowakowski, B. Peng, and R.J. Wyman. 1997. Patterns of connectivity in a *Drosophila* nerve. *J. Comp. Neurol*. 387:63–72. https://doi.org/10.1002/(SICI)1096-9861(19971013)387:1<63::AID-CNE6>3.0.CO;2-L

Elder, G.A., V.L. Friedrich, Jr., P. Bosco, C. Kang, A. Gourov, P.H. Tu, V.M. Lee, and R.A. Lazzarini. 1998. Absence of the mid-sized neurofilament subunit decreases axonal calibers, levels of light neurofilament (NF-L), and neurofilament content. *J. Cell Biol*. 141:727–739. https://doi.org/10.1083/jcb.141.3.727

Elfvin, L.G.. 1961. The ultrastructure of the nodes of Ranvier in cat sympathetic nerve fibers. *J. Ultrastruct. Res*. 5:374–387. https://doi.org/10.1016/S0022-5320(61)80014-2

Evans, M.D., A.S. Dumitrescu, D.L.H. Kruijssen, S.E. Taylor, and M.S. Grubb. 2015. Rapid modulation of axon initial segment length influences repetitive spike firing. *Cell Reports*. 13:1233–1245. https://doi.org/10.1016/j.celrep.2015.09.066

Evans, M.D., C. Tufo, A.S. Dumitrescu, and M.S. Grubb. 2017. Myosin II activity is required for structural plasticity at the axon initial segment. *Eur. J. Neurosci*. 46:1751–1757. https://doi.org/10.1111/ejn.13597

Eyer, J., D.W. Cleveland, P.C. Wong, and A.C. Peterson. 1998. Pathogenesis of two axonopathies does not require axonal neurofilaments. *Nature*. 391:584–587. https://doi.org/10.1038/35378

Eyer, J., and A. Peterson. 1994. Neurofilament-deficient axons and perikaryal aggregates in viable transgenic mice expressing a neurofilament-beta-galactosidase fusion protein. *Neuron*. 12:389–405. https://doi.org/10.1016/0896-6273(94)90280-1

Fadić, R., J. Vergara, and J. Alvarez. 1985. Microtubules and caliber of central and peripheral processes of sensory axons. *J. Comp. Neurol*. 236:258–264. https://doi.org/10.1002/cne.902360209

Farías, G.G., C.M. Guardia, D.J. Britt, X. Guo, and J.S. Bonifacino. 2015. Sorting of dendritic and axonal vesicles at the pre-axonal exclusion zone. *Cell Reports*. 13:1221–1232. https://doi.org/10.1016/j.celrep.2015.09.074

Fath, K.R., and R.J. Lasek. 1988. Two classes of actin microfilaments are associated with the inner cytoskeleton of axons. *J. Cell Biol*. 107:613–621. https://doi.org/10.1083/jcb.107.2.613

Foelix, R., and E. Hebets. 2001. Sensory biology of whip spiders (Arachnida, Amblypygi). Andrias. 15:129–140.

Foelix, R.F., and D. Troyer. 1980. Giant neurons and associated synapses in the peripheral nervous system of whip spiders. *J. Neurocytol*. 9:517–535. https://doi.org/10.1007/BF01204840

Fréal, A., D. Rai, R.P. Tas, X. Pan, E.A. Katrukha, D. van de Willige, R. Stucchi, A. Aher, C. Yang, A.F.M. Altelaar, et al. 2019. Feedback-Driven Assembly of the Axon Initial Segment. *Neuron*. 104:305–321.e8. https://doi.org/10.1016/j.neuron.2019.07.029

Friede, R.L.. 1971. Changes in microtubules and neurofilaments in constricted, hypoplastic nerve fibers. *Acta Neuropathol*. 5(Suppl 5):5 –: 216–225.

Friede, R.L., M. Benda, A. Dewitz, and P. Stoll. 1984. Relations between axon length and axon caliber. "Is maximum conduction velocity the factor controlling the evolution of nerve structure"? *J. Neurol. Sci*. 63:369–380. https://doi.org/10.1016/0022-510X(84)90160-6

Friede, R.L., T. Miyaghishi, and K.H. Hu. 1971. Axon calibre, neurofilaments, microtubules, sheath thickness and cholesterol in cat optic nerve fibres. *J. Anat*. 108:365–373.

Friede, R.L., and T. Samorajski. 1970. Axon caliber related to neurofilaments and microtubules in sciatic nerve fibers of rats and mice. *Anat. Rec*. 167:379–387. https://doi.org/10.1002/ar.1091670402

Garcia, M.L., C.S. Lobsiger, S.B. Shah, T.J. Deerinck, J. Crum, D. Young, C.M. Ward, T.O. Crawford, T. Gotow, Y. Uchiyama, et al. 2003. NF-M is an essential target for the myelin-directed "outside-in" signaling cascade that mediates radial axonal growth. *J. Cell Biol*. 163:1011–1020. https://doi.org/10.1083/jcb.200308159

Goldstein, R.H., O. Barkai, A. Íñigo-Portugués, B. Katz, S. Lev, and A.M. Binshtok. 2019. Location and plasticity of the sodium spike initiation zone in nociceptive terminals in vivo. *Neuron*. 102:801–812.e5. https://doi.org/10.1016/j.neuron.2019.03.005

Gonatas, N.K., and E. Robbins. 1965. The homology of spindle tubules and neuro-tubules in the chick embryo retina. *Protoplasma*. 59:377–391. https://doi.org/10.1007/BF01252447

González, C., and A. Couve. 2014. The axonal endoplasmic reticulum and protein trafficking: Cellular bootlegging south of the soma. *Semin. Cell Dev. Biol*. 27:23–31. https://doi.org/10.1016/j.semcdb.2013.12.004

Griffin, J.W., K.E. Fahnestock, D.L. Price, and P.N. Hoffman. 1983a. Microtubule-neurofilament segregation produced by beta, beta'-iminodipropionitrile: evidence for the association of fast axonal transport with microtubules. *J. Neurosci*. 3:557–566. https://doi.org/10.1523/JNEUROSCI.03-03-00557.1983

Griffin, J.W., K.E. Fahnestock, D.L. Price, and L.C. Cork. 1983b. Cytoskeletal disorganization induced by local application of beta, beta'-iminodipropionitrile and 2,5-hexanedione. *Ann. Neurol*. 14:55–61. https://doi.org/10.1002/ana.410140109

Grubb, M.S., and J. Burrone. 2010. Activity-dependent relocation of the axon initial segment fine-tunes neuronal excitability. *Nature*. 465:1070–1074. https://doi.org/10.1038/nature09160

Gumy, L.F., E.A. Katrukha, I. Grigoriev, D. Jaarsma, L.C. Kapitein, A. Akhmanova, and C.C. Hoogenraad. 2017. MAP2 Defines a Pre-axonal Filtering Zone to Regulate KIF1- versus KIF5-Dependent Cargo Transport in Sensory Neurons. *Neuron*. 94:347–362.e7. https://doi.org/10.1016/j.neuron.2017.03.046

Günay, C., F.H. Sieling, L. Dharmar, W.-H. Lin, V. Wolfram, R. Marley, R.A. Baines, and A.A. Prinz. 2015. Distal spike initiation zone location estimation by morphological simulation of ionic current filtering demonstrated in a novel model of an identified Drosophila motoneuron. *PLOS Comput. Biol*. 11. e1004189. https://doi.org/10.1371/journal.pcbi.1004189

Hahn, I., Y. Qu, M. Lees, J. Parkin, and A. Prokop. 2016. Novel concepts of microtubule regulation during neuronal growth, maintenance and degeneration. *In* Gordon-Kenan Research Seminar: Cell Biology of the Neuron. S. Meltzer and N. Khatri, editors, Waterville Valley, NH.

Hahn, I., A. Voelzmann, Y.-T. Liew, B. Costa-Gomes, and A. Prokop. 2019. The model of local axon homeostasis - explaining the role and regulation of microtubule bundles in axon maintenance and pathology. *Neural Dev*. 14:11. https://doi.org/10.1186/s13064-019-0134-0

Hamdan, H., B.C. Lim, T. Torii, A. Joshi, M. Konning, C. Smith, D.J. Palmer, P. Ng, C. Leterrier, J.A. Oses-Prieto, et al. 2020. Mapping axon initial segment structure and function by multiplexed proximity

biotinylation. *Nat. Commun.* 11:100. https://doi.org/10.1038/s41467-019-13658-5

Hámori, J., T. Pasik, and P. Pasik. 1978. Electron-microscopic identification of axonal initial segments belonging to interneurons in the dorsal lateral geniculate nucleus of the monkey. *Neuroscience.* 3:403–412. https://doi.org/10.1016/0306-4522(78)90042-8

Harada, A., K. Oguchi, S. Okabe, J. Kuno, S. Terada, T. Ohshima, R. Sato-Yoshitake, Y. Takei, T. Noda, and N. Hirokawa. 1994. Altered microtubule organization in small-calibre axons of mice lacking tau protein. *Nature.* 369:488–491. https://doi.org/10.1038/369488a0

Harterink, M., K. Vocking, X. Pan, E.M. Soriano Jerez, L. Slenders, A. Fréal, R.P. Tas, W.J. van de Wetering, K. Timmer, J. Motshagen, et al. 2019. TRIM46 organizes microtubule fasciculation in the axon initial segment. *J. Neurosci.* 39:4864–4873. https://doi.org/10.1523/JNEUROSCI.3105-18.2019

Hatch, R.J., Y. Wei, D. Xia, and J. Götz. 2017. Hyperphosphorylated tau causes reduced hippocampal CA1 excitability by relocating the axon initial segment. *Acta Neuropathol.* 133:717–730. https://doi.org/10.1007/s00401-017-1674-1

He, L., R. Kooistra, R. Das, E. Oudejans, E. van Leen, J. Ziegler, S. Portegies, B. de Haan, A. van Regteren Altena, R. Stucchi, et al. 2020. Cortical anchoring of the microtubule cytoskeleton is essential for neuron polarity. *Elife.* 9. . https://doi.org/10.7554/eLife.55111

Hedstrom, K.L., Y. Ogawa, and M.N. Rasband. 2008. AnkyrinG is required for maintenance of the axon initial segment and neuronal polarity. *J. Cell Biol.* 183:635–640. https://doi.org/10.1083/jcb.200806112

Hefting, L.L., E. D'Este, E. Arvedsen, T. Benned-Jensen, and H.B. Rasmussen. 2020. Multiple domains in the Kv7.3 C-terminus can regulate localization to the axon initial segment. *Front. Cell. Neurosci.* 14:10. https://doi.org/10.3389/fncel.2020.00010

Herrmann, H., and U. Aebi. 2016. Intermediate Filaments: Structure and Assembly. *Cold Spring Harb. Perspect. Biol.* 8. a018242. https://doi.org/10.1101/cshperspect.a018242

Hinds, J.W., and T.L. Ruffett. 1973. Mitral cell development in the mouse olfactory bulb: reorientation of the perikaryon and maturation of the axon initial segment. *J. Comp. Neurol.* 151:281–306. https://doi.org/10.1002/cne.901510305

Hirokawa, N.. 1982. Cross-linker system between neurofilaments, microtubules, and membranous organelles in frog axons revealed by the quick-freeze, deep-etching method. *J. Cell Biol.* 94:129–142. https://doi.org/10.1083/jcb.94.1.129

Hirokawa, N. 1991. Molecular architecture and dynamics of the neuronal cytoskeleton. *In* The neuronal cytoskeleton. R. Burgoyne, editor. Wiley-Liss, New York. 5–74.

Hirokawa, N., G.S. Bloom, and R.B. Vallee. 1985. Cytoskeletal architecture and immunocytochemical localization of microtubule-associated proteins in regions of axons associated with rapid axonal transport: the beta,beta'-iminodipropionitrile-intoxicated axon as a model system. *J. Cell Biol.* 101:227–239. https://doi.org/10.1083/jcb.101.1.227

Hirokawa, N., M.A. Glicksman, and M.B. Willard. 1984. Organization of mammalian neurofilament polypeptides within the neuronal cytoskeleton. *J. Cell Biol.* 98:1523–1536. https://doi.org/10.1083/jcb.98.4.1523

Hirokawa, N., S. Niwa, and Y. Tanaka. 2010. Molecular motors in neurons: transport mechanisms and roles in brain function, development, and disease. *Neuron.* 68:610–638. https://doi.org/10.1016/j.neuron.2010.09.039

Hoffman, P.N., J.W. Griffin, and D.L. Price. 1984. Control of axonal caliber by neurofilament transport. *J. Cell Biol.* 99:705–714. https://doi.org/10.1083/jcb.99.2.705

Hsieh, S.T., G.J. Kidd, T.O. Crawford, Z. Xu, W.M. Lin, B.D. Trapp, D.W. Cleveland, and J.W. Griffin. 1994. Regional modulation of neurofilament organization by myelination in normal axons. *J. Neurosci.* 14:6392–6401. https://doi.org/10.1523/JNEUROSCI.14-11-06392.1994

Huang, C.Y.-M., and M.N. Rasband. 2018. Axon initial segments: structure, function, and disease. *Ann. N. Y. Acad. Sci.* 1420:46–61. https://doi.org/10.1111/nyas.13718

Hummel, T., K. Krukkert, J. Roos, G. Davis, and C. Klämbt. 2000. Drosophila Futsch/22C10 is a MAP1B-like protein required for dendritic and axonal development. *Neuron.* 26:357–370. https://doi.org/10.1016/S0896-6273(00)81169-1

Ishikawa, H., S. Tsukita, and S. Tsukita. 1980. Arrangement of microtubules in rat peripheral myelinated axons. *Acta Anatomica Nipponica.* 55:441–442.

Jacko, M., S.M. Weyn-Vanhentenryck, J.W. Smerdon, R. Yan, H. Feng, D.J. Williams, J. Pai, K. Xu, H. Wichterle, and C. Zhang. 2018. Rbfox splicing factors promote neuronal maturation and axon initial segment assembly. *Neuron.* 97:853–868.

Jacomy, H., Q. Zhu, S. Couillard-Després, J.M. Beaulieu, and J.P. Julien. 1999. Disruption of type IV intermediate filament network in mice lacking the neurofilament medium and heavy subunits. *J. Neurochem.* 73:972–984. https://doi.org/10.1046/j.1471-4159.1999.0730972.x

Janmey, P.A., J.-F. Leterrier, and H. Herrmann. 2003. Assembly and structure of neurofilaments. *Curr. Opin. Colloid Interface Sci.* 8:40–47. https://doi.org/10.1016/S1359-0294(03)00010-4

Janning, D., M. Igaev, F. Sündermann, J. Brühmann, O. Beutel, J.J. Heinisch, L. Bakota, J. Piehler, W. Junge, and R. Brandt. 2014. Single-molecule tracking of tau reveals fast kiss-and-hop interaction with microtubules in living neurons. *Mol. Biol. Cell.* 25:3541–3551. https://doi.org/10.1091/mbc.e14-06-1099

Jenkins, P.M., N. Kim, S.L. Jones, W.C. Tseng, T.M. Svitkina, H.H. Yin, and V. Bennett. 2015. Giant ankyrin-G: a critical innovation in vertebrate evolution of fast and integrated neuronal signaling. *Proc. Natl. Acad. Sci. USA.* 112:957–964. https://doi.org/10.1073/pnas.1416544112

Jones, D.G. 1993. Electron microscopic exploration of synaptic organization. *In* Techniques in the Behavioral and Neural Sciences. Vol. 11. S.H. Parvez, M. Naoi, T. Nagatsu, and S. Parvez, editors. Elsevier, New York. 185–218.

Jones, E.G., and T.P. Powell. 1969. Synapses on the axon hillocks and initial segments of pyramidal cell axons in the cerebral cortex. *J. Cell Sci.* 5:495–507.

Jones, S.L., F. Korobova, and T. Svitkina. 2014. Axon initial segment cytoskeleton comprises a multiprotein submembranous coat containing sparse actin filaments. *J. Cell Biol.* 205:67–81. https://doi.org/10.1083/jcb.201401045

Jones, S.L., and T.M. Svitkina. 2016. Axon initial segment cytoskeleton: architecture, development, and role in neuron polarity. *Neural Plast.* 2016. 6808293. https://doi.org/10.1155/2016/6808293

Kang, J.-S., J.-H. Tian, P.-Y. Pan, P. Zald, C. Li, C. Deng, and Z.-H. Sheng. 2008. Docking of axonal mitochondria by syntaphilin controls their mobility and affects short-term facilitation. *Cell.* 132:137–148. https://doi.org/10.1016/j.cell.2007.11.024

Kemp, J.M., and T.P. Powell. 1971a. The structure of the caudate nucleus of the cat: light and electron microscopy. *Philos. Trans. R. Soc. Lond. B Biol. Sci.* 262:383–401. https://doi.org/10.1098/rstb.1971.0102

Kemp, J.M., and T.P. Powell. 1971b. The synaptic organization of the caudate nucleus. *Philos. Trans. R. Soc. Lond. B Biol. Sci.* 262:403–412. https://doi.org/10.1098/rstb.1971.0103

King, D.G., and R.J. Wyman. 1980. Anatomy of the giant fibre pathway in *Drosophila*. I. Three thoracic components of the pathway. *J. Neurocytol.* 9:753–770. https://doi.org/10.1007/BF01205017

Kobayashi, T., B. Storrie, K. Simons, and C.G. Dotti. 1992. A functional barrier to movement of lipids in polarized neurons. *Nature.* 359:647–650. https://doi.org/10.1038/359647a0

Kohno, K.. 1964. Neurotubles Contained within the Dendrite and Axon of Purkinje Cell of Frog. *Bull. Tokyo Med. Dent. Univ.* 11:411–442.

Kojima, T., and K. Saito. 1970. A photographic presentation on the initial segment of an anterior horn neuron in the cat. *J. Electron Microsc. (Tokyo).* 19:384–385.

Kole, M.H.P., and G.J. Stuart. 2012. Signal processing in the axon initial segment. *Neuron.* 73:235–247. https://doi.org/10.1016/j.neuron.2012.01.007

Kordeli, E., S. Lambert, and V. Bennett. 1995. AnkyrinG. A new ankyrin gene with neural-specific isoforms localized at the axonal initial segment and node of Ranvier. *J. Biol. Chem.* 270:2352–2359. https://doi.org/10.1074/jbc.270.5.2352

Kornreich, M., E. Malka-Gibor, A. Laser-Azogui, O. Doron, H. Herrmann, and R. Beck. 2015. Composite bottlebrush mechanics: α-internexin fine-tunes neurofilament network properties. *Soft Matter.* 11:5839–5849. https://doi.org/10.1039/C5SM00662G

Kosaka, T. 1980a. The axon initial segment as a synaptic site: ultrastructure and synaptology of the initial segment of the pyramidal cell in the rat hippocampus (CA3 region). *J. Neurocytol.* 9:861–882. https://doi.org/10.1007/BF01205024

Kosaka, T. 1980b. Ruffed cell: a new type of neuron with a distinctive initial unmyelinated portion of the axon in the olfactory bulb of the goldfish (*Carassius auratus*): II. Fine structure of the ruffed cell. *J. Comp. Neurol.* 193:119–145. https://doi.org/10.1002/cne.901930109

Kosaka, T.. 1983. Axon initial segments of the granule cell in the rat dentate gyrus: synaptic contacts on bundles of axon initial segments. *Brain Res.* 274:129–134. https://doi.org/10.1016/0006-8993(83)90527-9

Kosaka, T., and K. Hama. 1979a. Pre- and post-synaptic character of the axon initial segment of the mitral cell of the goldfish olfactory bulb. *Brain Res.* 169:570–574. https://doi.org/10.1016/0006-8993(79)90406-2

Kosaka, T., and K. Hama. 1979b. Ruffed cell: a new type of neuron with a distinctive initial unmyelinated portion of the axon in the olfactory bulb of the goldfish (*Carassius auratus*) I. Golgi impregnation and serial thin sectioning studies. *J. Comp. Neurol.* 186:301–319. https://doi.org/10.1002/cne.901860302

Kosaka, T., M. Komada, and K. Kosaka. 2008. Sodium channel cluster, betaIV-spectrin and ankyrinG positive "hot spots" on dendritic segments of parvalbumin-containing neurons and some other neurons in the mouse and rat main olfactory bulbs. *Neurosci. Res.* 62:176–186. https://doi.org/10.1016/j.neures.2008.08.002

Kreutzberg, G.W., and G.W. Gross. 1977. General morphology and axonal ultrastructure of the olfactory nerve of the pike, *Esox lucius*. *Cell Tissue Res.* 181:443–457. https://doi.org/10.1007/BF00221767

Kriebel, M., J. Metzger, S. Trinks, D. Chugh, R.J. Harvey, K. Harvey, and H. Volkmer. 2011. The cell adhesion molecule neurofascin stabilizes axo-axonic GABAergic terminals at the axon initial segment. *J. Biol. Chem.* 286:24385–24393. https://doi.org/10.1074/jbc.M110.212191

Krieg, M., J. Stühmer, J.G. Cueva, R. Fetter, K. Spilker, D. Cremers, K. Shen, A.R. Dunn, and M.B. Goodman. 2017. Genetic defects in β-spectrin and tau sensitize *C. elegans* axons to movement-induced damage via torque-tension coupling. *eLife*. 6. e20172. https://doi.org/10.7554/eLife.20172

Križ, J., Q. Zhu, J.P. Julien, and A.L. Padjen. 2000. Electrophysiological properties of axons in mice lacking neurofilament subunit genes: disparity between conduction velocity and axon diameter in absence of NF-H. *Brain Res.* 885: 32–44. https://doi.org/10.1016/S0006-8993(00)02899-7

Kuba, H., R. Adachi, and H. Ohmori. 2014. Activity-dependent and activity-independent development of the axon initial segment. *J. Neurosci.* 34: 3443–3453. https://doi.org/10.1523/JNEUROSCI.4357-13.2014

Kuba, H., Y. Oichi, and H. Ohmori. 2010. Presynaptic activity regulates Na(+) channel distribution at the axon initial segment. *Nature*. 465:1075–1078. https://doi.org/10.1038/nature09087

Kuba, H., R. Yamada, G. Ishiguro, and R. Adachi. 2015. Redistribution of Kv1 and Kv7 enhances neuronal excitability during structural axon initial segment plasticity. *Nat. Commun.* 6:8815. https://doi.org/10.1038/ncomms9815

Kubota, Y., J. Sohn, and Y. Kawaguchi. 2018. Large Volume Electron Microscopy and Neural Microcircuit Analysis. *Front. Neural Circuits*. 12:98. https://doi.org/10.3389/fncir.2018.00098

Kuijpers, M., D. van de Willige, A. Freal, A. Chazeau, M.A. Franker, J. Hofenk, R.J. Rodrigues, L.C. Kapitein, A. Akhmanova, D. Jaarsma, et al. 2016. Dynein regulator NDEL1 controls polarized cargo transport at the axon initial segment. *Neuron*. 89:461–471. https://doi.org/10.1016/j.neuron.2016.01.022

Kumar, S., and J.H. Hoh. 2004. Modulation of repulsive forces between neurofilaments by sidearm phosphorylation. *Biochem. Biophys. Res. Commun.* 324:489–496. https://doi.org/10.1016/j.bbrc.2004.09.076

Kurup, N., D. Yan, A. Goncharov, and Y. Jin. 2015. Dynamic microtubules drive circuit rewiring in the absence of neurite remodeling. *Curr. Biol.* 25:1594–1605. https://doi.org/10.1016/j.cub.2015.04.061

Kurup, N., Y. Li, A. Goncharov, and Y. Jin. 2018. Intermediate filament accumulation can stabilize microtubules in *Caenorhabditis elegans* motor neurons. *Proc. Natl. Acad. Sci. USA*. 115:3114–3119. https://doi.org/10.1073/pnas.1721930115

Lane, N.J., and N.J. Abbott. 1975. The organization of the nervous system in the crayfish *Procambarus clarkii*, with emphasis on the blood-brain interface. *Cell Tissue Res.* 156:173–187. https://doi.org/10.1007/BF00221801

Lane, N.J., and J.E. Treherne. 1970. Lanthanum staining of neurotubules in axons from cockroach ganglia. *J. Cell Sci.* 7:217–231.

Larivière, R.C., M.D. Nguyen, A. Ribeiro-da-Silva, and J.P. Julien. 2002. Reduced number of unmyelinated sensory axons in peripherin null mice. *J. Neurochem.* 81:525–532. https://doi.org/10.1046/j.1471-4159.2002.00853.x

Lee, G., and R. Brandt. 1992. Microtubule-bundling studies revisited: is there a role for MAPs? *Trends Cell Biol.* 2:286–289. https://doi.org/10.1016/0962-8924(92)90106-W

Leeson, T.S., and G.W. Higgs. 1982. Lanthanum as an intracellular stain for electron microscopy. *Histochem. J.* 14(4):553–560. . https://doi.org/10.1007/bf01011888

Leterrier, C.. 2018. The axon initial segment: an updated viewpoint. *J. Neurosci.* 38:2135–2145. https://doi.org/10.1523/JNEUROSCI.1922-17.2018

Leterrier, C., P. Dubey, and S. Roy. 2017a. The nano-architecture of the axonal cytoskeleton. *Nat. Rev. Neurosci.* 18:713–726. https://doi.org/10.1038/nrn.2017.129

Leterrier, C., N. Clerc, F. Rueda-Boroni, A. Montersino, B. Dargent, and F. Castets. 2017b. Ankyrin G Membrane Partners Drive the Establishment and Maintenance of the Axon Initial Segment. *Front. Cell. Neurosci.* 11:6. https://doi.org/10.3389/fncel.2017.00006

Leterrier, C., J. Potier, G. Caillol, C. Debarnot, F. Rueda Boroni, and B. Dargent. 2015. Nanoscale architecture of the axon initial segment reveals an organized and robust scaffold. *Cell Reports*. 13:2781–2793. https://doi.org/10.1016/j.celrep.2015.11.051

Leterrier, J.F., R.K. Liem, and M.L. Shelanski. 1982. Interactions between neurofilaments and microtubule-associated proteins: a possible mechanism for intraorganellar bridging. *J. Cell Biol.* 95:982–986. https://doi.org/10.1083/jcb.95.3.982

Levavasseur, F., Q. Zhu, and J.P. Julien. 1999. No requirement of alpha-internexin for nervous system development and for radial growth of axons. *Brain Res. Mol. Brain Res.* 69:104–112. https://doi.org/10.1016/S0169-328X(99)00104-7

Lewis, T.L., Jr., T. Mao, K. Svoboda, and D.B. Arnold. 2009. Myosin-dependent targeting of transmembrane proteins to neuronal dendrites. *Nat. Neurosci.* 12:568–576. https://doi.org/10.1038/nn.2318

Lin, M.-Y., X.-T. Cheng, P. Tammineni, Y. Xie, B. Zhou, Q. Cai, and Z.-H. Sheng. 2017. Releasing syntaphilin removes stressed mitochondria from axons independent of mitophagy under pathophysiological conditions. *Neuron*. 94:595–610.e6. https://doi.org/10.1016/j.neuron.2017.04.004

Liu, C.H., S.R. Stevens, L.H. Teliska, M. Stankewich, P.J. Mohler, T.J. Hund, and M.N. Rasband. 2020. Nodal β spectrins are required to maintain Na^+ channel clustering and axon integrity. *eLife*. 9. e52378. https://doi.org/10.7554/eLife.52378

Machnicka, B., A. Czogalla, A. Hryniewicz-Jankowska, D.M. Bogusławska, R. Grochowalska, E. Heger, and A.F. Sikorski. 2014. Spectrins: a structural platform for stabilization and activation of membrane channels, receptors and transporters. *Biochim. Biophys. Acta*. 1838:620–634. https://doi.org/10.1016/j.bbamem.2013.05.002

Malbouisson, A.M., M.N. Ghabriel, and G. Allt. 1985. Axonal microtubules: a computer-linked quantitative analysis. *Anat. Embryol. (Berl.)*. 171:339–344. https://doi.org/10.1007/BF00347022

Marner, L., J.R. Nyengaard, Y. Tang, and B. Pakkenberg. 2003. Marked loss of myelinated nerve fibers in the human brain with age. *J. Comp. Neurol.* 462:144–152. https://doi.org/10.1002/cne.10714

Marygold, S.J., M.A. Crosby, and J.L. Goodman; FlyBase Consortium. 2016. Using FlyBase, a database of Drosophila genes and genomes. *Methods Mol. Biol.* 1478:1–31. https://doi.org/10.1007/978-1-4939-6371-3_1

Matsumura, A., and K. Kohno. 1991. Microtubule bundles in fish cerebellar Purkinje cells. *Anat. Embryol. (Berl.)*. 183:105–110. https://doi.org/10.1007/BF00174390

Matus, A.. 1991. Microtubule-associated proteins and neuronal morphogenesis. *J. Cell Sci. Suppl.* 15(Supplement 15):61–67. https://doi.org/10.1242/jcs.1991.Supplement_15.9

Méphon-Gaspard, A., M. Boca, C. Pioche-Durieu, B. Desforges, A. Burgo, L. Hamon, O. Piétrement, and D. Pastré. 2016. Role of tau in the spatial organization of axonal microtubules: keeping parallel microtubules evenly distributed despite macromolecular crowding. *Cell. Mol. Life Sci.* 73:3745–3760. https://doi.org/10.1007/s00018-016-2216-z

Mikhaylova, M., B.M. Cloin, K. Finan, R. van den Berg, J. Teeuw, M.M. Kijanka, M. Sokolowski, E.A. Katrukha, M. Maidorn, F. Opazo, et al. 2015. Resolving bundled microtubules using anti-tubulin nanobodies. *Nat. Commun.* 6:7933. https://doi.org/10.1038/ncomms8933

Miller, R.H., R.J. Lasek, and M.J. Katz. 1987. Preferred microtubules for vesicle transport in lobster axons. *Science*. 235:220–222. https://doi.org/10.1126/science.2432661

Miyata, Y., M. Hoshi, E. Nishida, Y. Minami, and H. Sakai. 1986. Binding of microtubule-associated protein 2 and tau to the intermediate filament reassembled from neurofilament 70-kDa subunit protein. Its regulation by calmodulin. *J. Biol. Chem.* 261:13026–13030.

Monaco, S., L. Autilio-Gambetti, R.J. Lasek, M.J. Katz, and P. Gambetti. 1989. Experimental increase of neurofilament transport rate: decreases in neurofilament number and in axon diameter. *J. Neuropathol. Exp. Neurol.* 48:23–32. https://doi.org/10.1097/00005072-198901000-00003

Monroy, B.Y., D.L. Sawyer, B.E. Ackermann, M.M. Borden, T.C. Tan, and K.M. Ori-McKenney. 2018. Competition between microtubule-associated proteins directs motor transport. *Nat. Commun.* 9:1487. https://doi.org/10.1038/s41467-018-03909-2

Monroy, B.Y., T.C. Tan, J.M. Oclaman, J.S. Han, S. Simó, S. Niwa, D.W. Nowakowski, R.J. McKenney, and K.M. Ori-McKenney. 2020. A combinatorial MAP code dictates polarized microtubule transport. *Dev. Cell*. 53:60–72.e4. https://doi.org/10.1016/j.devcel.2020.01.029

Nadelhaft, I.. 1974. Microtubule densities and total numbers in selected axons of the crayfish abdominal nerve cord. *J. Neurocytol.* 3:73–86. https://doi.org/10.1007/BF01111933

Nakada, C., K. Ritchie, Y. Oba, M. Nakamura, Y. Hotta, R. Iino, R.S. Kasai, K. Yamaguchi, T. Fujiwara, and A. Kusumi. 2003. Accumulation of anchored proteins forms membrane diffusion barriers during neuronal polarization. *Nat. Cell Biol.* 5:626–632. https://doi.org/10.1038/ncb1009

Nakajima, Y.. 1974. Fine structure of the synaptic endings on the Mauthner cell of the goldfish. *J. Comp. Neurol.* 156:379–402. https://doi.org/10.1002/cne.901560402

Nakazawa, E., and H. Ishikawa. 1995. Occurrence of fasciculated microtubules at nodes of Ranvier in rat spinal roots. *J. Neurocytol.* 24:399–407. https://doi.org/10.1007/BF01189066

Nascimento, A.I., F.M. Mar, and M.M. Sousa. 2018. The intriguing nature of dorsal root ganglion neurons: Linking structure with polarity and function. *Prog. Neurobiol.* 168:86–103. https://doi.org/10.1016/j.pneurobio.2018.05.002

Nixon, R.A., P.A. Paskevich, R.K. Sihag, and C.Y. Thayer. 1994. Phosphorylation on carboxyl terminus domains of neurofilament proteins in retinal ganglion cell neurons in vivo: influences on regional neurofilament accumulation, interneurofilament spacing, and axon caliber. *J. Cell Biol.* 126:1031–1046. https://doi.org/10.1083/jcb.126.4.1031

Ochs, R.L., and P.R. Burton. 1980. Distribution and selective extraction on filamentous components associated with axonal microtubules of crayfish nerve cord. *J. Ultrastruct. Res.* 73:169–182. https://doi.org/10.1016/S0022-5320(80)90122-7

Ochs, S., J. Erdman, R.A. Jersild, Jr., and V. McAdoo. 1978. Routing of transported materials in the dorsal root and nerve fiber branches of the dorsal root ganglion. *J. Neurobiol.* 9:465–481. https://doi.org/10.1002/neu.480090606

Ohara, O., Y. Gahara, T. Miyake, H. Teraoka, and T. Kitamura. 1993. Neurofilament deficiency in quail caused by nonsense mutation in neurofilament-L gene. *J. Cell Biol.* 121:387–395. https://doi.org/10.1083/jcb.121.2.387

Palay, S.L., C. Sotelo, A. Peters, and P.M. Orkand. 1968. The axon hillock and the initial segment. *J. Cell Biol.* 38:193–201. https://doi.org/10.1083/jcb.38.1.193

Pan-Vazquez, A., W. Wefelmeyer, V. Gonzalez Sabater, G. Neves, and J. Burrone. 2020. Activity-Dependent Plasticity of Axo-axonic Synapses at the Axon Initial Segment. *Neuron.* 106:1–12.

Pannese, E., G. Arcidiacono, L. Rigamonti, P. Procacci, and M. Ledda. 1982. Stability at low temperatures of neuronal microtubules in spinal ganglia and dorsal roots of the lizard (*Lacerta muralis*). *J. Ultrastruct. Res.* 79:18–30. https://doi.org/10.1016/S0022-5320(82)90049-1

Pannese, E., M. Ledda, G. Arcidiacono, L. Rigamonti, and P. Procacci. 1981. Density and distribution of microtubules in the axons of the lizard dorsal roots. *J. Submicrosc. Cytol.* 13:169–181.

Pannese, E., M. Ledda, G. Arcidiacono, L. Rigamonti, and P. Procacci. 1984. A comparison of the density of microtubules in the central and peripheral axonal branches of the pseudounipolar neurons of lizard spinal ganglia. *Anat. Rec.* 208:595–605. https://doi.org/10.1002/ar.1092080415

Papasozomenos, S.C., L. Autilio-Gambetti, and P. Gambetti. 1981. Reorganization of axoplasmic organelles following beta, beta'-iminodipropionitrile administration. *J. Cell Biol.* 91:866–871. https://doi.org/10.1083/jcb.91.3.866

Papasozomenos, S.C., L.I. Binder, P.K. Bender, and M.R. Payne. 1985. Microtubule-associated protein 2 within axons of spinal motor neurons: associations with microtubules and neurofilaments in normal and beta,beta'-iminodipropionitrile-treated axons. *J. Cell Biol.* 100:74–85. https://doi.org/10.1083/jcb.100.1.74

Parhad, I.M., A.W. Clark, and J.W. Griffin. 1987. Effect of changes in neurofilament content on caliber of small axons: the beta,beta'-iminodipropionitrile model. *J. Neurosci.* 7:2256–2263. https://doi.org/10.1523/JNEUROSCI.07-07-02256.1987

Paul, D.M., J. Mantell, U. Borucu, J. Coombs, K.J. Surridge, J.M. Squire, P. Verkade, and M.P. Dodding. 2019. In situ cryo-electron tomography reveals filamentous actin within the microtubule lumen. *bioRxiv*. doi: 10.1101/844043 (Preprint posted November 18, 2019)

Peach, R.. 1975. Tubules and filaments in satellite cells and axons of sensory neurons. *Am. J. Anat.* 142:385–390. https://doi.org/10.1002/aja.1001420307

Perge, J.A., K. Koch, R. Miller, P. Sterling, and V. Balasubramanian. 2009. How the optic nerve allocates space, energy capacity, and information. *J. Neurosci.* 29:7917–7928. https://doi.org/10.1523/JNEUROSCI.5200-08.2009

Perge, J.A., J.E. Niven, E. Mugnaini, V. Balasubramanian, and P. Sterling. 2012. Why do axons differ in caliber? *J. Neurosci.* 32:626–638. https://doi.org/10.1523/JNEUROSCI.4254-11.2012

Perrot, R., R. Berges, A. Bocquet, and J. Eyer. 2008. Review of the multiple aspects of neurofilament functions, and their possible contribution to neurodegeneration. *Mol. Neurobiol.* 38:27–65. https://doi.org/10.1007/s12035-008-8033-0

Peter, A., and R. Stick. 2015. Evolutionary aspects in intermediate filament proteins. *Curr. Opin. Cell Biol.* 32:48–55. https://doi.org/10.1016/j.ceb.2014.12.009

Peters, A.. 1966. The node of Ranvier in the central nervous system. *Q. J. Exp. Physiol. Cogn. Med. Sci.* 51:229–236.

Peters, A., S.L. Palay, and H. Webster. 1991. The Fine Structure of the Nervous System: Neurons and Their Supporting Cells. Oxford University Press, New York, Oxford.

Peters, A., C.C. Proskauer, and I.R. Kaiserman-Abramof. 1968. The small pyramidal neuron of the rat cerebral cortex. The axon hillock and initial segment. *J. Cell Biol.* 39:604–619. https://doi.org/10.1083/jcb.39.3.604

Pinching, A.J., and T.P. Powell. 1971. The neuron types of the glomerular layer of the olfactory bulb. *J. Cell Sci.* 9:305–345.

Polilov, A.A.. 2012. The smallest insects evolve anucleate neurons. *Arthropod Struct. Dev.* 41:29–34.

Poritsky, R.. 1969. Two and three dimenstional ultrastructure of boutons and glial cells on the motoneuronal surface in the cat spinal cord. *J. Comp. Neurol.* 135:423–452. https://doi.org/10.1002/cne.901350404

Price, R.L., P. Paggi, R.J. Lasek, and M.J. Katz. 1988. Neurofilaments are spaced randomly in the radial dimension of axons. *J. Neurocytol.* 17:55–62. https://doi.org/10.1007/BF01735377

Price, J.L., and T.P. Powell. 1970. The mitral and short axon cells of the olfactory bulb. *J. Cell Sci.* 7:631–651.

Qu, Y., I. Hahn, S.E.D. Webb, S.P. Pearce, and A. Prokop. 2017. Periodic actin structures in neuronal axons are required to maintain microtubules. *Mol. Biol. Cell.* 28:296–308. https://doi.org/10.1091/mbc.e16-10-0727

Raine, C.S., B. Ghetti, and M.L. Shelanski. 1971. On the association between microtubules and mitochondria within axons. *Brain Res.* 34:389–393. https://doi.org/10.1016/0006-8993(71)90293-9

Rao, M.V., M.L. Garcia, Y. Miyazaki, T. Gotow, A. Yuan, S. Mattina, C.M. Ward, N.A. Calcutt, Y. Uchiyama, R.A. Nixon, et al. 2002. Gene replacement in mice reveals that the heavily phosphorylated tail of neurofilament heavy subunit does not affect axonal caliber or the transit of cargoes in slow axonal transport. *J. Cell Biol.* 158:681–693. https://doi.org/10.1083/jcb.200202037

Reles, A., and R.L. Friede. 1991. Axonal cytoskeleton at the nodes of Ranvier. *J. Neurocytol.* 20:450–458. https://doi.org/10.1007/BF01252273

Rice, R.V., P.F. Roslansky, N. Pascoe, and S.M. Houghton. 1980. Bridges between microtubules and neurofilaments visualized by stereoelectron microscopy. *J. Ultrastruct. Res.* 71:303–310. https://doi.org/10.1016/S0022-5320(80)90081-7

Rodríguez Echandía, E.L., R.S. Piezzi, and E.M. Rodríguez. 1968. Dense-core microtubules in neurons and gliocytes of the toad Bufo arenarum Hensel. *Am. J. Anat.* 122:157–166. https://doi.org/10.1002/aja.1001220110

Rolls, M.M.. 2011. Neuronal polarity in *Drosophila*: sorting out axons and dendrites. *Dev. Neurobiol.* 71:419–429. https://doi.org/10.1002/dneu.20836

Rosenberg, K.J., J.L. Ross, H.E. Feinstein, S.C. Feinstein, and J. Israelachvili. 2008. Complementary dimerization of microtubule-associated tau protein: Implications for microtubule bundling and tau-mediated pathogenesis. *Proc. Natl. Acad. Sci. USA.* 105:7445–7450. https://doi.org/10.1073/pnas.0802036105

Saito, K.. 1972. The initial segment of DSCT (dorsal spino-cerebellar tract) neurons in the cat. *J. Electron Microsc. (Tokyo).* 21:325–326.

Sakaguchi, T., M. Okada, T. Kitamura, and K. Kawasaki. 1993. Reduced diameter and conduction velocity of myelinated fibers in the sciatic nerve of a neurofilament-deficient mutant quail. *Neurosci. Lett.* 153:65–68. https://doi.org/10.1016/0304-3940(93)90078-Y

Salzer, J.L.. 2019. An unfolding role for ankyrin-G at the axon initial segment. *Proc. Natl. Acad. Sci. USA.* 116:19228–19230. https://doi.org/10.1073/pnas.1914002116

Samsonov, A., J.Z. Yu, M. Rasenick, and S.V. Popov. 2004. Tau interaction with microtubules in vivo. *J. Cell Sci.* 117:6129–6141. https://doi.org/10.1242/jcs.01531

Sánchez-Huertas, C., F. Freixo, R. Viais, C. Lacasa, E. Soriano, and J. Lüders. 2016. Non-centrosomal nucleation mediated by augmin organizes microtubules in post-mitotic neurons and controls axonal microtubule polarity. *Nat. Commun.* 7:12187. https://doi.org/10.1038/ncomms12187

Sánchez-Soriano, N., W. Bottenberg, A. Fiala, U. Haessler, A. Kerassoviti, E. Knust, R. Löhr, and A. Prokop. 2005. Are dendrites in *Drosophila* homologous to vertebrate dendrites? *Dev. Biol.* 288:126–138. https://doi.org/10.1016/j.ydbio.2005.09.026

Sánchez-Soriano, N., M. Travis, F. Dajas-Bailador, C. Gonçalves-Pimentel, A.J. Whitmarsh, and A. Prokop. 2009. Mouse ACF7 and drosophila short stop modulate filopodia formation and microtubule organisation during neuronal growth. *J. Cell Sci.* 122:2534–2542. https://doi.org/10.1242/jcs.046268

Satake, T., K. Yamashita, K. Hayashi, S. Miyatake, M. Tamura-Nakano, H. Doi, Y. Furuta, G. Shioi, E. Miura, Y.H. Takeo, et al. 2017. MTCL1 plays an essential role in maintaining Purkinje neuron axon initial segment. *EMBO J.* 36:1227–1242. https://doi.org/10.15252/embj.201695630

Schlüter, A., S. Rossberger, D. Dannehl, J.M. Janssen, S. Vorwald, J. Hanne, C. Schultz, D. Mauceri, and M. Engelhardt. 2019. Dynamic regulation of synaptopodin and the axon initial segment in retinal ganglion cells during postnatal development. *Front. Cell. Neurosci.* 13:318. https://doi.org/10.3389/fncel.2019.00318

Schnapp, B.J., and T.S. Reese. 1982. Cytoplasmic structure in rapid-frozen axons. *J. Cell Biol.* 94:667–669. https://doi.org/10.1083/jcb.94.3.667

Shaklai, M., and M. Tavassoli. 1982. Lanthanum as an electron microscopic stain. *J. Histochem. Cytochem.* 30(12):1325–1330. . https://doi.org/10.1177/30.12.6185564

Shi, L., S. Yi, and Y. Li. 2018. Genome survey sequencing of red swamp crayfish *Procambarus clarkii*. *Mol. Biol. Rep.* 45:799–806. https://doi.org/10.1007/s11033-018-4219-3

Sloper, J.J., and T.P. Powell. 1973. Observations on the axon initial segment and other structures in the neocortex using conventional staining and ethanolic phosphotungstic acid. *Brain Res.* 50:163–169. https://doi.org/10.1016/0006-8993(73)90602-1

Sloper, J.J., and T.P. Powell. 1979. A study of the axon initial segment and proximal axon of neurons in the primate motor and somatic sensory cortices. *Philos. Trans. R. Soc. Lond. B Biol. Sci.* 285:173–197. https://doi.org/10.1098/rstb.1979.0004

Smarandache-Wellmann, C.R.. 2016. Arthropod neurons and nervous system. *Curr. Biol.* 26:R960–R965. https://doi.org/10.1016/j.cub.2016.07.063

Smith, D.H.. 2009. Stretch growth of integrated axon tracts: extremes and exploitations. *Prog. Neurobiol.* 89:231–239. https://doi.org/10.1016/j.pneurobio.2009.07.006

Smith, D.S., U. Järlfors, and R. Beránek. 1970. The organization of synaptic axcplasm in the lamprey (petromyzon marinus) central nervous system. *J. Cell Biol.* 46:199–219. https://doi.org/10.1083/jcb.46.2.199

Smith, D.S., U. Järlfors, and B.F. Cameron. 1975. Morphological evidence for the participation of microtubules in axonal transport. *Ann. N. Y. Acad. Sci.* 253(1 The Biology o):472–506. https://doi.org/10.1111/j.1749-6632.1975.tb19223.x

Smith, D.S., U. Järlfors, and M.L. Cayer. 1977. Structural cross-bridges between microtubules and mitochondria in central axons of an insect (*Periplaneta americana*). *J. Cell Sci.* 27:255–272.

Smith, R.S.. 1973. Microtubule and neurofilament densities in amphibian spinal root nerve fibers: relationship to axoplasmic transport. *Can. J. Physiol. Pharmacol.* 51:798–806. https://doi.org/10.1139/y73-123

Sobotzik, J.-M., J.M. Sie, C. Politi, D. Del Turco, V. Bennett, T. Deller, and C. Schultz. 2009. AnkyrinG is required to maintain axo-dendritic polarity in vivo. *Proc. Natl. Acad. Sci. USA.* 106:17564–17569. https://doi.org/10.1073/pnas.0909267106

Sohn, P.D., C.T. Huang, R. Yan, L. Fan, T.E. Tracy, C.M. Camargo, K.M. Montgomery, T. Arhar, S.A. Mok, R. Freilich, et al. 2019. Pathogenic tau impairs axon initial segment plasticity and excitability homeostasis. *Neuron.* 104:458–470.e5. https://doi.org/10.1016/j.neuron.2019.08.008

Somogyi, P., T.F. Freund, and A. Cowey. 1982. The axo-axonic interneuron in the cerebral cortex of the rat, cat and monkey. *Neuroscience.* 7:2577–2607. https://doi.org/10.1016/0306-4522(82)90086-0

Song, Y., L.L. Kirkpatrick, A.B. Schilling, D.L. Helseth, N. Chabot, J.W. Keillor, G.V. Johnson, and S.T. Brady. 2013. Transglutaminase and polyamination of tubulin: posttranslational modification for stabilizing axonal microtubules. *Neuron.* 78:109–123. https://doi.org/10.1016/j.neuron.2013.01.036

Sotelo, C., and S.L. Palay. 1968. The fine structure of the lateral vestibular nucleus in the rat. I. Neurons and neuroglial cells. *J. Cell Biol.* 36:151–179. https://doi.org/10.1083/jcb.36.1.151

Stephan, R., B. Goellner, E. Moreno, C.A. Frank, T. Hugenschmidt, C. Genoud, H. Aberle, and J. Pielage. 2015. Hierarchical microtubule organization controls axon caliber and transport and determines synaptic structure and stability. *Dev. Cell.* 33:5–21. https://doi.org/10.1016/j.devcel.2015.02.003

Stevens, M.J., and J.H. Hoh. 2010. Conformational dynamics of neurofilament side-arms. *J. Phys. Chem. B.* 114:8879–8886. https://doi.org/10.1021/jp102128u

Stiess, M., N. Maghelli, L.C. Kapitein, S. Gomis-Rüth, M. Wilsch-Bräuninger, C.C. Hoogenraad, I.M. Tolić-Nørrelykke, and F. Bradke. 2010. Axon extension occurs independently of centrosomal microtubule nucleation. *Science.* 327:704–707. https://doi.org/10.1126/science.1182179

Svitkina, T.M., A.B. Verkhovsky, and G.G. Borisy. 1996. Plectin sidearms mediate interaction of intermediate filaments with microtubules and other components of the cytoskeleton. *J. Cell Biol.* 135:991–1007. https://doi.org/10.1083/jcb.135.4.991

Szaro, B.G., and M.J. Strong. 2010. Post-transcriptional control of neurofilaments: New roles in development, regeneration and neurodegenerative disease. *Trends Neurosci.* 33:27–37. https://doi.org/10.1016/j.tins.2009.10.002

Tanner, K.D., J.D. Levine, and K.S. Topp. 1998. Microtubule disorientation and axonal swelling in unmyelinated sensory axons during vincristine-induced painful neuropathy in rat. *J. Comp. Neurol.* 395:481–492. https://doi.org/10.1002/(SICI)1096-9861(19980615)395:4<481::AID-CNE5>3.0.CO;2-Y

Tas, R.P., A. Chazeau, B.M.C. Cloin, M.L.A. Lambers, C.C. Hoogenraad, and L.C. Kapitein. 2017. Differentiation between oppositely oriented microtubules controls polarized neuronal transport. *Neuron.* 96:1264–1271.e5. https://doi.org/10.1016/j.neuron.2017.11.018

Tsukita, S., and H. Ishikawa. 1976. Three-dimensional distribution of smooth endoplasmic reticulum in myelinated axons. *J. Electron Microsc. (Tokyo).* 25:141–149.

Tsukita, S., and H. Ishikawa. 1981. The cytoskeleton in myelinated axons: serial section study. *Biochem. Res. (Tokyo).* 2:424–437.

Tsukita, S., J. Usukura, S. Tsukita, and H. Ishikawa. 1982. The cytoskeleton in myelinated axons: a freeze-etch replica study. *Neuroscience.* 7:2135–2147. https://doi.org/10.1016/0306-4522(82)90125-7

van Beuningen, S.F.B., L. Will, M. Harterink, A. Chazeau, E.Y. van Battum, C.P. Frias, M.A.M. Franker, E.A. Katrukha, R. Stucchi, K. Vocking, et al. 2015. TRIM46 controls neuronal polarity and axon specification by driving the formation of parallel microtubule arrays. *Neuron.* 88:1208–1226. https://doi.org/10.1016/j.neuron.2015.11.012

Vassilopoulos, S., S. Gibaud, A. Jimenez, G. Caillol, and C. Leterrier. 2019. Ultrastructure of the axonal periodic scaffold reveals a braid-like organization of actin rings. *Nat. Commun.* 10:5803. https://doi.org/10.1038/s41467-019-13835-6

Viancour, T.A., K.R. Seshan, G.D. Bittner, and R.A. Sheller. 1987. Organization of axoplasm in crayfish giant axons. *J. Neurocytol.* 16:557–566. https://doi.org/10.1007/BF01668508

Villarroel-Campos, D., and C. Gonzalez-Billault. 2014. The MAP1B case: an old MAP that is new again. *Dev. Neurobiol.* 74:953–971. https://doi.org/10.1002/dneu.22178

Voelzmann, A., Y.-T. Liew, Y. Qu, I. Hahn, C. Melero, N. Sánchez-Soriano, and A. Prokop. 2017. Drosophila Short stop as a paradigm for the role and regulation of spectraplakins. *Semin. Cell Dev. Biol.* 69:40–57. https://doi.org/10.1016/j.semcdb.2017.05.019

Warren, R.H.. 1984. Axonal microtubules of crayfish and spiny lobster nerve cords are decorated with a heat-stable protein of high molecular weight. *J. Cell Sci.* 71:1–15.

Watanabe, K., S. Al-Bassam, Y. Miyazaki, T.J. Wandless, P. Webster, and D.B. Arnold. 2012. Networks of polarized actin filaments in the axon initial segment provide a mechanism for sorting axonal and dendritic proteins. *Cell Reports.* 2:1546–1553. https://doi.org/10.1016/j.celrep.2012.11.015

Waxman, S.G., G.D. Pappas, and M.V. Bennett. 1972. Morphological correlates of functional differentiation of nodes of Ranvier along single fibers in the neurogenic electric organ of the knife fish *Stern archus*. *J. Cell Biol.* 53:210–224. https://doi.org/10.1083/jcb.53.1.210

Willey, T.J.. 1973. The ultrastructure of the cat olfactory bulb. *J. Comp. Neurol.* 152:211–232. https://doi.org/10.1002/cne.901520302

Weaver, D.J., and T.A. Viancour. 1991. The crayfish neuronal cytoskeleton: an investigation of proteins having neurofilament-like immunoreactivity. *Brain Res.* 544:49–58. https://doi.org/10.1016/0006-8993(91)90884-X

Weaver, D.J., and T.A. Viancour. 1992. A crustacean neuronal cytoskeletal protein with characteristics of neurofilaments and microtubule-associated proteins. *J. Comp. Neurol.* 320:110–120. https://doi.org/10.1002/cne.903200108

Weiss, P.A., and R. Mayr. 1971a. Neuronal organelles in neuroplasmic ("axonal") flow. II. Neurotubules. *Acta Neuropathol.* 5(Suppl 5):5: 198–20.

Weiss, P.A., and R. Mayr. 1971b. Organelles in neuroplasmic ("axonal") flow: neurofilaments. *Proc. Natl. Acad. Sci. USA.* 68:846–850. https://doi.org/10.1073/pnas.68.4.846

Westrum, L.E.. 1970. Observations on initial segments of axons in the prepyriform cortex of the rat. *J. Comp. Neurol.* 139:337–356. https://doi.org/10.1002/cne.901390306

Winckler, B., P. Forscher, and I. Mellman. 1999. A diffusion barrier maintains distribution of membrane proteins in polarized neurons. *Nature*. 397: 698–701. https://doi.org/10.1038/17806

Wortman, J.C., U.M. Shrestha, D.M. Barry, M.L. Garcia, S.P. Gross, and C.C. Yu. 2014. Axonal transport: how high microtubule density can compensate for boundary effects in small-caliber axons. *Biophys. J.* 106: 813–823. https://doi.org/10.1016/j.bpj.2013.12.047

Wouterlood, F.G., and E. Mugnaini. 1984. Cartwheel neurons of the dorsal cochlear nucleus: a Golgi-electron microscopic study in rat. *J. Comp. Neurol.* 227:136–157. https://doi.org/10.1002/cne.902270114

Wuerker, R.B., and S.L. Palay. 1969. Neurofilaments and microtubules in anterior horn cells of the rat. *Tissue Cell*. 1:387–402. https://doi.org/10.1016/S0040-8166(69)80012-1

Xu, C.S., K.J. Hayworth, Z. Lu, P. Grob, A.M. Hassan, J.G. García-Cerdán, K.K. Niyogi, E. Nogales, R.J. Weinberg, and H.F. Hess. 2017. Enhanced FIB-SEM systems for large-volume 3D imaging. *eLife*. 6. e25916. https://doi.org/10.7554/eLife.25916

Xu, K., G. Zhong, and X. Zhuang. 2013. Actin, spectrin, and associated proteins form a periodic cytoskeletal structure in axons. *Science*. 339: 452–456. https://doi.org/10.1126/science.1232251

Xu, Z., J.R. Marszalek, M.K. Lee, P.C. Wong, J. Folmer, T.O. Crawford, S.T. Hsieh, J.W. Griffin, and D.W. Cleveland. 1996. Subunit composition of neurofilaments specifies axonal diameter. *J. Cell Biol.* 133:1061–1069. https://doi.org/10.1083/jcb.133.5.1061

Xue, C., B. Shtylla, and A. Brown. 2015. A stochastic multiscale model that explains the segregation of axonal microtubules and neurofilaments in neurological diseases. *PLOS Comput. Biol.* 11:e1004406–e1004406. https://doi.org/10.1371/journal.pcbi.1004406

Yamasaki, H., G.S. Bennett, C. Itakura, and M. Mizutani. 1992. Defective expression of neurofilament protein subunits in hereditary hypotrophic axonopathy of quail. *Lab. Invest.* 66:734–743.

Yamasaki, H., C. Itakura, and M. Mizutani. 1991. Hereditary hypotrophic axonopathy with neurofilament deficiency in a mutant strain of the Japanese quail. *Acta Neuropathol.* 82:427–434. https://doi.org/10.1007/BF00293376

Yang, R., K.K. Walder-Christensen, N. Kim, D. Wu, D.N. Lorenzo, A. Badea, Y.-H. Jiang, H.H. Yin, W.C. Wetsel, and V. Bennett. 2019. *ANK2* autism mutation targeting giant ankyrin-B promotes axon branching and ectopic connectivity. *Proc. Natl. Acad. Sci. USA*. 116:15262–15271. https://doi.org/10.1073/pnas.1904348116

Yang, Y., Y. Ogawa, K.L. Hedstrom, and M.N. Rasband. 2007. betaIV spectrin is recruited to axon initial segments and nodes of Ranvier by ankyrinG. *J. Cell Biol.* 176:509–519. https://doi.org/10.1083/jcb.200610128

Yau, K.W., P. Schätzle, E. Tortosa, S. Pagès, A. Holtmaat, L.C. Kapitein, and C.C. Hoogenraad. 2016. Dendrites in vitro and in vivo contain microtubules of opposite polarity and axon formation correlates with uniform plus-end-out microtubule orientation. *J. Neurosci.* 36:1071–1085. https://doi.org/10.1523/JNEUROSCI.2430-15.2016

Ye, J., J. Li, F. Ye, Y. Zhang, M. Zhang, and C. Wang. 2020. Mechanistic insights into the interactions of dynein regulator Ndel1 with neuronal ankyrins and implications in polarity maintenance. *Proc. Natl. Acad. Sci. USA*. 117:1207–1215. https://doi.org/10.1073/pnas.1916987117

Yin, X., T.O. Crawford, J.W. Griffin, P. Tu, V.M. Lee, C. Li, J. Roder, and B.D. Trapp. 1998. Myelin-associated glycoprotein is a myelin signal that modulates the caliber of myelinated axons. *J. Neurosci.* 18:1953–1962. https://doi.org/10.1523/JNEUROSCI.18-06-01953.1998

Yogev, S., R. Cooper, R. Fetter, M. Horowitz, and K. Shen. 2016. Microtubule organization determines axonal transport dynamics. *Neuron*. 92: 449–460. https://doi.org/10.1016/j.neuron.2016.09.036

Young, J.. 1936. The giant nerve fibres and epistellar body of cephalopods. *Q. J. Microsc. Sci.* 78:367–386.

Yu, W., F.J. Ahmad, and P.W. Baas. 1994. Microtubule fragmentation and partitioning in the axon during collateral branch formation. *J. Neurosci.* 14:5872–5884. https://doi.org/10.1523/JNEUROSCI.14-10-05872.1994

Yu, W., and P.W. Baas. 1994. Changes in microtubule number and length during axon differentiation. *J. Neurosci.* 14:2818–2829. https://doi.org/10.1523/JNEUROSCI.14-05-02818.1994

Yuan, A., T. Sasaki, A. Kumar, C.M. Peterhoff, M.V. Rao, R.K. Liem, J.P. Julien, and R.A. Nixon. 2012. Peripherin is a subunit of peripheral nerve neurofilaments: implications for differential vulnerability of CNS and peripheral nervous system axons. *J. Neurosci.* 32:8501–8508. https://doi.org/10.1523/JNEUROSCI.1081-12.2012

Yum, S.W., J. Zhang, K. Mo, J. Li, and S.S. Scherer. 2009. A novel recessive Nefl mutation causes a severe, early-onset axonal neuropathy. *Ann. Neurol.* 66:759–770. https://doi.org/10.1002/ana.21728

Zelená, J.. 1971. Neurofilaments and microtubules in sensory neurons after peripheral nerve section. *Z. Zellforsch. Mikrosk. Anat.* 117:191–211. https://doi.org/10.1007/BF00330737

Zenker, W., and E. Högl. 1976. The prebifurcation section of the axon of the rat spinal ganglion cell. *Cell Tissue Res.* 165:345–363. https://doi.org/10.1007/BF00222438

Zenker, W., and E. Hohberg. 1973. A-α-nerve-fiber: number of neurotubules in the stem fibre and in the terminal branches. *J. Neurocytol.* 2:143–148. https://doi.org/10.1007/BF01474716

Zenker, W., R. Mayr, and H. Gruber. 1973. Axoplasmic organelles: quantitative differences between ventral and dorsal root fibres of the rat. *Experientia*. 29:77–78. https://doi.org/10.1007/BF01913263

Zenker, W., R. Mayr, and H. Gruber. 1975. Neurotubules: different densities in peripheral motor and sensory nerve fibres. *Experientia*. 31:318–320. https://doi.org/10.1007/BF01922561

Zhu, Q., S. Couillard-Després, and J.P. Julien. 1997. Delayed maturation of regenerating myelinated axons in mice lacking neurofilaments. *Exp. Neurol.* 148:299–316. https://doi.org/10.1006/exnr.1997.6654

Zhu, Q., M. Lindenbaum, F. Levavasseur, H. Jacomy, and J.-P. Julien. 1998. Disruption of the NF-H gene increases axonal microtubule content and velocity of neurofilament transport: relief of axonopathy resulting from the toxin β,β′-iminodipropionitrile. *J. Cell Biol.* 143:183–193. https://doi.org/10.1083/jcb.143.1.183

Supplemental material

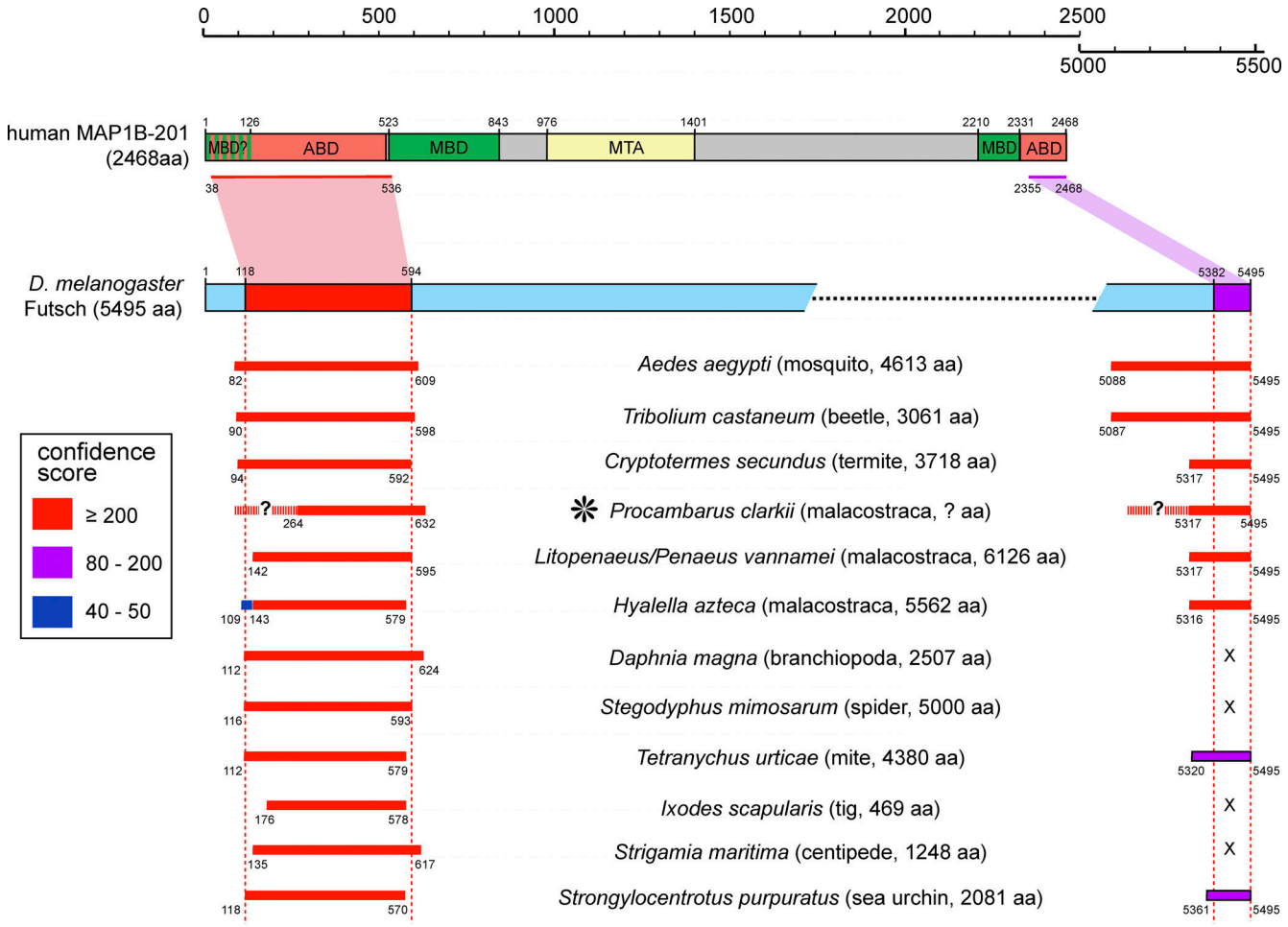

Figure S1. **Homology of *Drosophila* Futsch to human MAP1B and Futsch-like genes in other invertebrates.** Human MAP1B is shown at the top; borders of functional domains were taken from the 9-aa-shorter rat gene (Villarroel-Campos and Gonzalez-Billault, 2014): ABD, actin-binding domain; MBD, MT-binding domain; MTA, MT assembly-helping domain. The *Drosophila* Futsch gene is shown below, indicating the homologous regions shared with human MAP1B. The bars further below indicate homologies of other invertebrate Fusch-like genes, mapped onto the *Drosophila* Futsch gene; asterisk indicates the crayfish homologue mentioned in the main text. All sequences were blasted against the *D. melanogaster* genome using the blastp 2.2.18 tool provided in FlyBase (Altschul et al., 1997; Marygold et al., 2016). In all cases, Futsch was identified as the only stringent homologue, with the areas of homology all coinciding in the same N- and C-terminal regions as indicated in the figure. The following sequences were used: human MAP1B-201, ensembl.org gene ENST00000296755.12; *D. melanogaster* Futsch, ensembl.org gene FBpp0300235; *Procambarus clarkii*, extracted by Llilians Calvo-González (University of Manchester, Manchester, UK) from nonassembled genomic sequence kindly provided by Yanhe Li (Huazhong Agricultural University, Wuhan, People's Republic of China; Shi et al., 2018); *Aedes aegypti*, VectorBase gene AAEL009847-RB; *Tribolium castaneum*, ensembl.org gene TC001001_001; *Cryptotermes secundus*, NCBI gene XP_023712736.1; *(Lito)penaeus vannamei*, NCBI gene XP_027226604.1; *Hyalella azteca*, NCBI gene XP_018026291.1; *Daphnia magna*, ensembl.org gene APZ42_014156; *Stegodyphus mimosarum*, ensembl.org gene X975_00566; *Tetranychus urticae*, NCBI gene XP_015781552.1; *Ixodes scapularis*, VectorBase gene ISCW009767-RA; *Strigamia maritima*, ensembl.org gene SMAR006539-RA; and *Strongylocentrotus purpuratus*, ensembl.org gene SP-MAP1APH

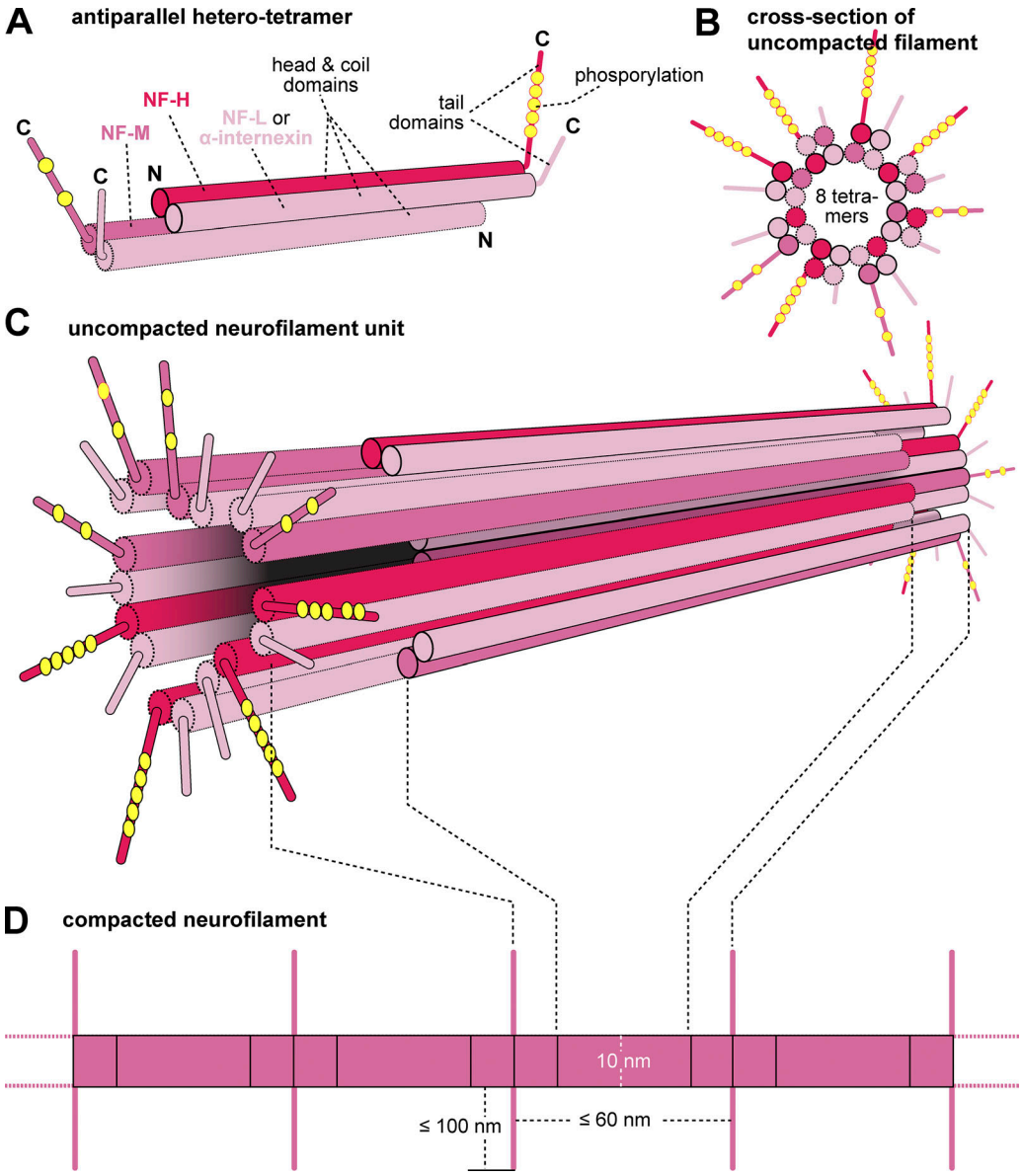

Figure S2. **Composition of NFs. (A)** Usually, NF-M or NF-H forms parallel heterodimers with NF-L, which, in turn, arrange into antiparallel heterotetramers through partial overlap of their coiled domains, explaining the lack of polarity in NFs. **(B)** Eight tetramers assemble into a unit, with the tail domains sticking out further aided by phosphorylation of the M- and H-tails (tail domains of the NF proteins with stippled outlines are left out for clarity). **(C)** 3D view of the same unit as shown in B, now displaying all tail domains; note that inside-out orientation of tetramers is randomized, since it seems unknown whether this property follows a strict order in real filaments. **(D)** Proposed dimensions in assembled filaments where units are radially compacted and annealed end to end. Information for this model was taken from Janmey et al., 2003; Kornreich et al., 2015; Szaro and Strong, 2010.

Tables S1 and S2 are provided online as separate PDF files. In Table S1, the second and third columns show diameters and lengths of AISs (where mentioned). The fourth column shows properties of AISs; apart from periglomerular cells, all AISs display dense undercoats (DUCs) and MT fascicles (MTFs); many AISs display cisternae (C) or cisternal organs (COs) that tend to be close to synaptic contacts or synaptic spine-like processes (SLP); according to Peters et al., 1991 (pp. 152 and 176), type I/asymmetric synapses with round clear vesicles are considered excitatory, whereas type II/symmetric synapses with flat or pleiotropic clear vesicles are inhibitory. Abbreviations used: IS, OS, RS, and NS represent input, output, reciprocal, and no synapses; –1/–2, asymmetric/symmetric synapse; and –FV, –PV, and –RV represent flat, pleiotropic, and round vesicles); axons of ruffed cells display an unconventional initial unmyelinated portion (IP; Fig. 2 F), of which only the most proximal part displays all AIS features. The fifth column shows the source. In Table S2, data were extracted from graphs and/or texts of the various publications; they indicate highest and lowest values as a crude representation of data ranges, whereas more specific analyses and correlations could not be

considered here. Values without brackets were taken from those publications, whereas data in brackets were calculated in retrospect on the basis of presented data. Footnote and abbreviations: (1) reduced by organelle area (~15%); n.d., not determined. Information sources as indicated in the tables: Kohno, 1964; Andres, 1965a; Palay et al., 1968; Peters et al., 1968; Sotelo and Palay, 1968; Conradi, 1969; Conradi and Skoglund, 1969; Jones and Powell, 1969; Poritsky, 1969; Friede and Samorajski, 1970; Kojima and Saito, 1970; Price and Powell, 1970; Westrum, 1970; Friede, 1971; Friede et al., 1971; Kemp and Powell, 1971a, 1971b; Pinching and Powell, 1971; Weiss and Mayr, 1971b; Chan-Palay, 1972; Saito, 1972; Hinds and Ruffett, 1973; Sloper and Powell, 1973, 1979; Smith, 1973; Willey, 1973; Zenker and Hohberg, 1973; Zenker et al., 1973, 1975; Nadelhaft, 1974; Nakajima, 1974; Smith et al., 1975, 1977; Kreutzberg and Gross, 1977; Hámori et al., 1978; Ochs et al., 1978; Kosaka and Hama, 1979a, 1979b, Kosaka, 1980a, 1980b, 1983, Pannese et al., 1981, 1982, 1984; Alvarez et al., 1982; Somogyi et al., 1982; Hoffman et al., 1984; Wouterlood and Mugnaini, 1984; Fadić et al., 1985; Malbouisson et al., 1985; Viancour et al., 1987; Price et al., 1988; Monaco et al., 1989; de Zeeuw et al., 1990; Alfei et al., 1991; Reles and Friede, 1991; Harada et al., 1994; Elder et al., 1998; Tanner et al., 1998.